

# Ultrastrong coupling between light and matter

*Anton Frisk Kockum<sup>1,2\*</sup>, Adam Miranowicz<sup>1,3</sup>, Simone De Liberato<sup>4</sup>, Salvatore Savasta<sup>1,5</sup> and Franco Nori<sup>1,6\*</sup>*

**Abstract** | Ultrastrong coupling between light and matter has, in the past decade, transitioned from a theoretical idea to an experimental reality. It is a new regime of quantum light–matter interaction, which goes beyond weak and strong coupling to make the coupling strength comparable to the transition frequencies in the system. The achievement of weak and strong coupling has led to increased control of quantum systems and to applications such as lasers, quantum sensing, and quantum information processing. Here we review the theory of quantum systems with ultrastrong coupling, discussing entangled ground states with virtual excitations, new avenues for nonlinear optics, and connections to several important physical models. We also overview the multitude of experimental setups, including superconducting circuits, organic molecules, semiconductor polaritons, and optomechanical systems, that have now achieved ultrastrong coupling. We conclude by discussing the many potential applications that these achievements enable in physics and chemistry.

The intuitive description of the interaction between light and matter as a series of elementary processes in which a photon is absorbed, emitted or scattered by a distribution of charges essentially hinges on the small value of the fine structure constant  $\alpha \approx \frac{1}{137}$ . Because  $\alpha$  is the natural dimensionless parameter emerging in a perturbative treatment of quantum electrodynamics, its small value allows most of the quantum dynamics of the electromagnetic field to be described by only taking into account first-order (absorption, emission) or second-order (scattering) processes.

Whereas the value of  $\alpha$  is fixed by nature, Purcell discovered in 1946 that the strength of the interaction of an emitter with light can be enhanced or suppressed by engineering its electromagnetic environment<sup>1</sup>. From this crucial observation sprang a whole field of research, today called cavity quantum electrodynamics (QED; FIG. 1), which aims to exploit different kinds of photonic resonators to modulate the coupling of light with matter.

The fundamental and applied importance of controlling the strength of light–matter coupling,  $g$ , led to the development of resonators with ever higher quality factors,  $Q$ , which are associated with lower energy losses.

In 1983, Haroche and co-workers<sup>2</sup>, using a collection of Rydberg atoms in a high- $Q$  microwave cavity, managed to achieve a coupling strength that exceeded the losses in the system. In this strong-coupling (SC; FIG. 1d) regime it is possible to observe an oscillatory exchange of energy quanta between the matter and the light, called vacuum Rabi oscillations, which takes place at a

rate given by  $g$ . By contrast, in the weak-coupling (WC; FIG. 1c) regime  $g$  is smaller than the losses, and thus the energy is lost from the system before it can be exchanged between the light and the matter.

The SC regime was soon also reached with single atoms coherently interacting with a microwave cavity<sup>3</sup> and, a few years later, with an optical cavity<sup>4</sup>. In 1992, the SC regime was demonstrated using quasi-2D electronic excitations (Wannier excitons) embedded in a semiconductor optical microcavity<sup>5</sup>. In this case, the eigenstates of the resulting system are called cavity polaritons. Following these pioneering experiments, cavity QED has been successfully adapted and further developed using artificial atoms, such as quantum dots<sup>6</sup> and superconducting qubits (circuit QED)<sup>7</sup>.

In a cavity-QED setup, the dimensionless parameter quantifying the interaction is the ratio between the coupling strength  $g$  and the bare energy of the excitations. This quantity, the normalized coupling  $\eta$ , is proportional to a positive power of  $\alpha$  and its value in the first observations of the SC regime was  $<10^{-6}$  for atoms<sup>4</sup> and  $10^{-3}$  for Wannier excitons in semiconductor microcavities<sup>5</sup>. Lowest-order perturbation theory is thus perfectly adequate to describe those experiments. The important difference with the WC regime is that, because the coupling is larger than the spectral width of the excitations, degenerate perturbation theory needs to be applied.

It took more than two decades after the observation of SC for the cavity-QED community to begin

<sup>1</sup>Theoretical Quantum Physics Laboratory, RIKEN Cluster for Pioneering Research, Wako-shi, Saitama, Japan.

<sup>2</sup>Wallenberg Centre for Quantum Technology, Department of Microtechnology and Nanoscience, Chalmers University of Technology, Gothenburg, Sweden.

<sup>3</sup>Faculty of Physics, Adam Mickiewicz University, Poznań, Poland.

<sup>4</sup>School of Physics and Astronomy, University of Southampton, Southampton, UK.

<sup>5</sup>Dipartimento di Scienze Matematiche e Informatiche, Scienze Fisiche e Scienze della Terra, Università di Messina, Messina, Italy.

<sup>6</sup>Physics Department, University of Michigan, Ann Arbor, MI, USA.

\*e-mail: [anton.frisk.kockum@gmail.com](mailto:anton.frisk.kockum@gmail.com); [fnori@riken.jp](mailto:fnor@riken.jp)  
<https://doi.org/10.1038/s42254-018-0006-2>

**Key points**

- Ultrastrong coupling (USC) can be achieved by coupling many dipoles to light, or by using degrees of freedom whose coupling is not bounded by the smallness of the fine-structure constant.
- The highest light-matter coupling strengths have been measured in experiments with Landau polaritons in semiconductor systems and in setups with superconducting quantum circuits.
- With USC, standard approximations break down, allowing processes that do not conserve the number of excitations in the system, leading to a ground state that contains virtual excitations.
- Potential applications of USC include fast and protected quantum information processing, nonlinear optics, modified chemical reactions and the enhancement of various quantum phenomena.
- Now that USC has been reached in several systems, it is time to experimentally explore the new phenomena predicted for this regime and to find their useful applications.

investigating the possibility of accessing a regime with larger  $\eta$  in which higher-order processes, which would hybridize states with different numbers of excitations, become observable. Two main paths were identified to reach such a regime. The first consisted in coupling many dipoles to the same cavity mode (FIG. 1b); as correctly predicted by the Dicke model<sup>8</sup>, this leads to enhanced coupling that scales with the square root of the number of dipoles. The second path was to use different degrees of freedom, whose coupling is not bounded by the small value of  $\alpha$ . An in-depth discussion of the scaling of  $\eta$  with  $\alpha$  in different physical implementations can be found elsewhere<sup>9</sup>.

In 2005, following the first path, it was predicted<sup>10</sup> that this regime, which was named the ultrastrong-coupling (USC; FIG. 1e) regime, could be observed in intersubband polaritons thanks to the large number of electrons involved in the transitions between parallel subbands in a quantum well. In 2009, the USC regime was observed for the first time in a microcavity-embedded doped GaAs quantum well, with  $\eta = 0.11$  (REF.<sup>11</sup>). Following this initial observation, the value of  $\eta = 0.1$  has often been taken as a threshold for the USC regime. However, because the intensity of higher-order processes depends continuously on  $\eta$ , the value of 0.1 is just a historical convention, without any deeper physical meaning.

The second path has been followed in experiments with superconducting circuits<sup>7</sup>, in which USC was observed in 2010, with  $\eta = 0.10\text{--}0.12$  (REF.<sup>12,13</sup>). In these experiments, it becomes possible to explore the USC of light to a single two-level system, instead of a collective excitation.

Following these experimental breakthroughs, the interest in USC has blossomed, fostered by the vast phenomenology that has been predicted to be observable in this regime, including modifications of intensity, spectral features and correlations of light-emitting devices with USC<sup>14,15</sup>, as well as possible modifications of physical or chemical properties of systems ultrastrongly coupled to light<sup>10,16–20</sup>. This widespread interest led not only to the observation of the USC regime in a large number of physical systems, but also to a steady increase in normalized coupling, whose record is presently  $\eta = 1.43$  (REF.<sup>21</sup>).

The achievement of USC can be seen as the beginning of a third chapter in the history of light-matter interaction (FIG. 1). Already the control of this interaction afforded by the Purcell effect in the WC regime had led to several important applications, such as low-threshold solid-state lasers<sup>22</sup> and efficient single-photon and entangled-photon emitters<sup>23,24</sup>. Cavity QED with individual atoms in the SC regime made it possible to manipulate and control quantum systems, enabling tests of fundamental physics<sup>25</sup> and applications<sup>26</sup> such as high-precision measurements<sup>27</sup> and quantum information processing (QIP)<sup>28</sup>. As the light-matter coupling strength reaches the USC regime, it starts to become possible to modify the very nature of the light and matter degrees of freedom. This opens new avenues for studying and engineering non-perturbatively coupled light-matter systems, which is likely to lead to novel applications.

In this Review, we gather both theoretical insights and experimental achievements in the field of USC. We begin by discussing various regimes of light-matter coupling in more detail, explaining their similarities and differences, the models used to describe them and their properties. We then examine how USC has been reached in different experimental systems. This is followed by an overview of the defining characteristics of ultrastrong light-matter interaction such as virtual excitations and higher-order processes, which affect how the interaction of an USC system with an environment is treated. We also survey quantum simulations of the USC regime, USC to a continuum instead of a single resonator mode and how ultrastrong light-matter coupling is intimately connected to other areas of physics. We conclude with an outlook for the field, including possible new applications and outstanding challenges.

**Light-matter coupling regimes and models**

The definitions of the WC, SC and USC regimes compare the light-matter coupling strength  $g$  with different parameters (FIG. 1). Whether the coupling is strong or weak depends on whether  $g$  is larger than the losses in the system. USC is not SC with larger couplings; its definition does not involve the value of losses but instead compares  $g$  with bare energies in the system. It is thus possible for a system to be in the USC regime without having SC if losses are large<sup>29</sup>. The ratio  $\eta$  that defines USC instead determines whether perturbation theory can be used and to what extent approximations can be made in models for the light-matter interaction.

**Models.** Some of the most fundamental models describing light-matter interaction, the quantum Rabi, Dicke and Hopfield models, are described in BOX 1. These models do not approximate away some terms that are often ignored at low light-matter coupling strengths, but they still rely on various approximations, for example, they assume that the atoms are two-level systems and that the light is in a single mode. Recently, some of these approximations have been shown to become potentially unsound in the USC regime. Specifically, the inclusion of multiple modes

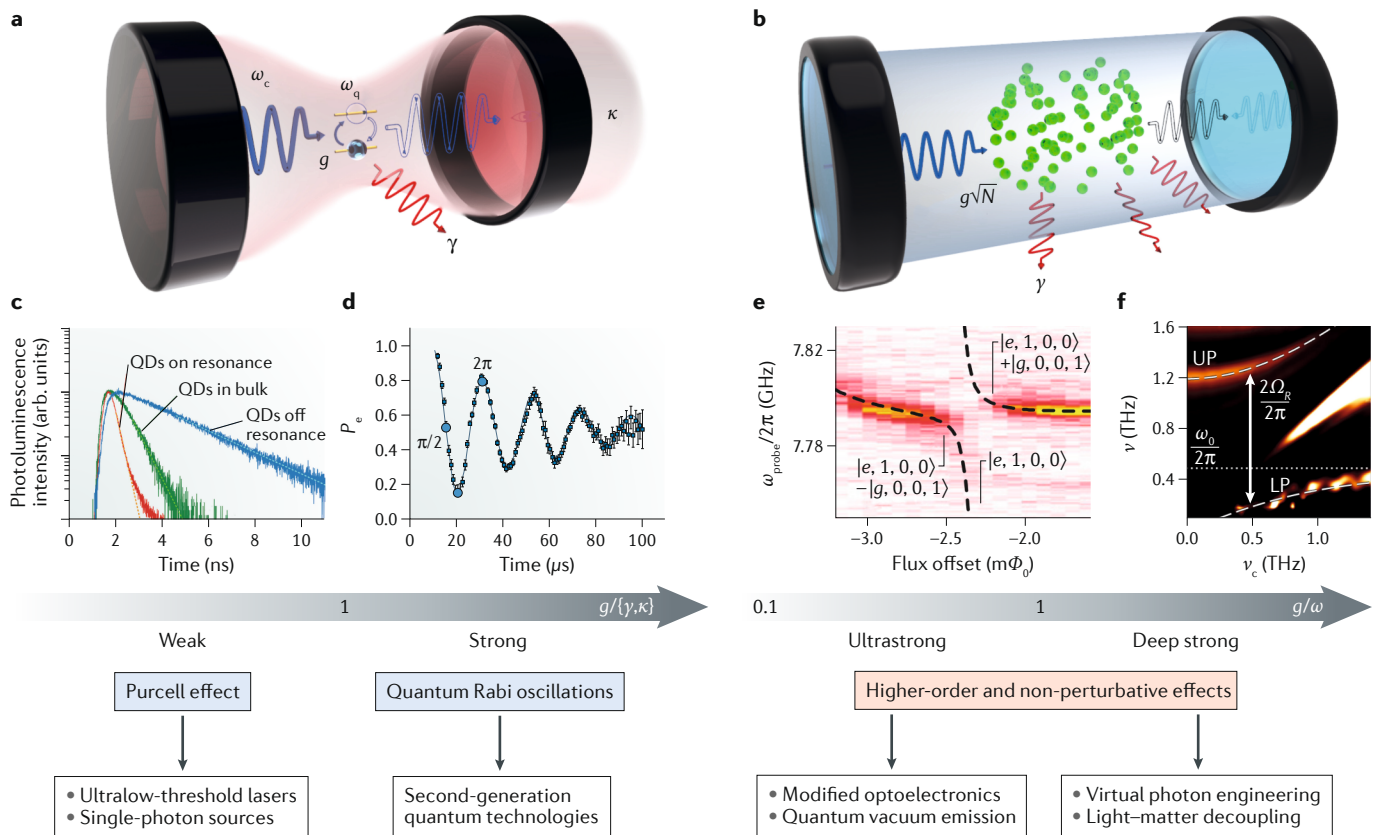


**Fig. 1 | Regimes of light-matter interaction.** **a** | Sketch of a cavity quantum electrodynamics (QEDs) system with a single two-level atom (qubit; the simplest example of a matter system). The parameters determining the different interaction regimes are the resonance frequency  $\omega_c$  of the cavity mode, the transition frequency  $\omega_q$  of the qubit, the coupling strength  $g$  and the cavity and qubit loss rates,  $\kappa$  and  $\gamma$ , respectively. **b** | Sketch of an optical resonator coupled to many quantum emitters. The light-matter coupling strength can be enhanced by increasing the number  $N$  of emitters interacting with the resonator. The resulting collective coupling strength scales as  $g\sqrt{N}$ .

**c–f** | Four representative cavity-QED experiments illustrating different light-matter interaction regimes. **c** | Weak coupling: experimental demonstration of full control of the spontaneous-emission dynamics of single quantum dots (QDs) by a photonic-crystal nanocavity<sup>216</sup>. The plot shows time-resolved micro-photoluminescence intensities of InGaAs QDs on resonance with the cavity, off resonance and in bulk without any cavity. Compared with the case without any cavity, the QDs decay more quickly in a resonant cavity (which enhances the density of states that the QDs can decay to) and more slowly in an off-resonant cavity (which shields the QD from the environment). This is the Purcell effect<sup>1</sup>.

**d** | Strong coupling: data from a pioneering experiment<sup>217</sup> with Rydberg atoms coupled to a superconducting microwave Fabry-Pérot resonator, displaying vacuum Rabi oscillations. An atom in the excited state  $|e\rangle$  enters an empty resonant cavity and the excitation is exchanged back and forth between the atom and the resonator before it decays.  $P_e$  denotes the probability of detecting the atom in  $|e\rangle$  as a function of the effective interaction time.

**e** | Ultrastrong coupling: microwave spectroscopy of a system with a superconducting flux qubit coupled to a coplanar-waveguide resonator<sup>12</sup>. The system displays a normalized coupling strength  $\eta = g/\omega_c = 0.12$ . The plot shows the cavity transmission as a function of probe frequency  $\omega_{\text{probe}}$  and flux offset, which tunes the qubit frequency. The avoided level crossing indicates a coupling between states with different numbers of excitations (one state has a single photon in the third resonator mode; the other state has one qubit excitation and one photon in the first resonator mode). Such a coupling requires counter-rotating terms and is not reproduced by the Jaynes-Cummings approximation (BOX 1).

**f** | Deep strong coupling: magneto-THz transmission measurements on a THz metamaterial coupled to the cyclotron resonance of a 2D electron gas<sup>21</sup>. The splitting  $2\Omega_R$  between the lower polariton (LP) and upper polariton (UP) levels that emerges as the cyclotron frequency  $\nu_c$  is tuned is a measure of the coupling strength. In this work, a record  $\eta = 1.43$  was reached.

**g** | Phenomena and applications associated with different strengths of light-matter interaction. Panel **c** is adapted with permission from REF.<sup>216</sup>, APS. Panel **d** is adapted with permission from REF.<sup>217</sup>, APS. Panel **e** is reproduced from REF.<sup>12</sup>, Springer Nature Limited. Panel **f** is reproduced with permission from REF.<sup>21</sup>, ACS.

of the photonic resonator has been shown to become a necessity at larger couplings<sup>30–34</sup>, leading to important changes in the system dynamics even for seemingly safe values of the normalized coupling<sup>35</sup>. It is also possible to have USC of matter to a continuum of light modes, a scenario discussed below. Moreover,

the validity of retaining a single optically active transition in the quantum description of the matter part of the system has recently been demonstrated to be strongly gauge-dependent<sup>36,37</sup>. This remains true even for very anharmonic potentials, in which all the higher-lying transitions are spectrally distant from the

## Box 1 | Models for light–matter coupling

The quantum Rabi model<sup>220</sup> is one of the simplest and most fundamental models of light–matter interaction. In the quantum Rabi model, the interaction between a single-mode bosonic field (such as a cavity mode with frequency  $\omega_c$ ) and a generic two-level system (or a qubit, with level splitting  $\omega_q$ ) is described by the quantum Rabi Hamiltonian ( $\hbar=1$ )

$$\hat{H}_{\text{Rabi}} = \omega_c \hat{a}^\dagger \hat{a} + \frac{1}{2} \omega_q \hat{\sigma}_z + \hat{H}_{\text{int}}, \quad (\text{B1.1})$$

$$\hat{H}_{\text{int}} = g \hat{X} \hat{\sigma}_x = g_1 (\hat{a} \hat{\sigma}_+ + \hat{a}^\dagger \hat{\sigma}_-) + g_2 (\hat{a} \hat{\sigma}_- + \hat{a}^\dagger \hat{\sigma}_+), \quad (\text{B1.2})$$

where  $\hat{a}$  and  $\hat{a}^\dagger$  are the annihilation and creation operators of the cavity mode, respectively;  $\hat{\sigma}_- = |g\rangle\langle e|$  and  $\hat{\sigma}_+ = |e\rangle\langle g|$  are the lowering and raising operators between the ground ( $|g\rangle$ ) and excited ( $|e\rangle$ ) states of a given two-level system;  $\hat{\sigma}_x = \hat{\sigma}_- + \hat{\sigma}_+$  and  $\hat{\sigma}_z = |e\rangle\langle e| - |g\rangle\langle g|$  are Pauli operators; and  $\hat{X} = \hat{a} + \hat{a}^\dagger$  is the canonical position operator of the electrical field of the cavity mode. For simplicity, we ignore the vacuum-field energy in the free Hamiltonian in equation B1.1.  $g_1$ ,  $g_2$  and  $g$  denote light–matter coupling strengths. In the quantum Rabi model,  $g = g_1 = g_2$ , but this condition can be relaxed<sup>221</sup>. Setting  $g_2 = 0$  gives the Jaynes–Cummings model<sup>39</sup>. The extensions of the quantum Rabi model and the Jaynes–Cummings model to multiple atoms are the Dicke<sup>8</sup> and Tavis–Cummings<sup>48</sup> models, respectively, as summarized in the table below.

A Rabi-type model can also be applied to describe the interaction between two coupled harmonic oscillators. This is an effective description of many systems in which the light is coupled not to a single atom or molecule, but to an ensemble of them. For example, the standard fermion–boson quantum Rabi model can be generalized to a purely bosonic multi-mode Hopfield model<sup>222</sup>, which describes the interaction between photons and collective excitations (such as plasmons or phonons) of a matter system. A simplified two-mode version of the Hopfield model is

$$\hat{H}_{\text{Hopfield}} = \omega_c \hat{a}^\dagger \hat{a} + \omega_b \hat{b}^\dagger \hat{b} + \hat{H}'_{\text{int}} + \hat{H}_{\text{dia}}, \quad (\text{B1.3})$$

$$\hat{H}'_{\text{int}} = g \hat{X} \hat{Y}' = ig_1 (\hat{a} \hat{b}^\dagger - \hat{a}^\dagger \hat{b}) + ig_2 (\hat{a}^\dagger \hat{b}^\dagger - \hat{a} \hat{b}), \quad (\text{B1.4})$$

where  $\hat{b}$  and  $\hat{b}^\dagger$  are the annihilation and creation operators, respectively, for collective excitations of a matter system of frequency  $\omega_b$ , and  $\hat{Y}' = i(\hat{b}^\dagger - \hat{b})$  is the quadrature corresponding to the canonical momentum operator of the matter mode. The Hamiltonian  $\hat{H}_{\text{dia}}$  describes the diamagnetic term (also referred to as the  $A^2$  term), which is proportional to  $\hat{X}^2$ . This term is also sometimes added to the standard quantum Rabi model. The physical meaning of  $\hat{H}_{\text{dia}}$ , and the conditions under which this term can be omitted, are discussed in BOX 2.

	1 atom	N atoms
Without RWA	Quantum Rabi model <sup>220</sup>	Dicke model <sup>8</sup> , Hopfield model <sup>222</sup>
With RWA	Jaynes–Cummings model <sup>39</sup>	Tavis–Cummings model <sup>48</sup>

RWA, rotating-wave approximation.

lowest one, a case in which this kind of approximation is generally considered to be safe<sup>37</sup>. To solve this issue, the introduction of a generalized minimal-coupling replacement has been proposed<sup>38</sup>, allowing the gauge-invariant Hamiltonians on the reduced Hilbert space to be derived.

The light–matter interaction can be divided into two parts (BOX 1). It is essential to note that, in contrast to the terms in the first part (weighted by the coupling strength  $g_1$ ), the terms in the second part (weighted by  $g_2$ ) do not conserve  $\hat{N}_{\text{exc}}$ , the total number of excitations in the system. These latter terms are often referred to as anti-resonant or counter-rotating. When the light and matter frequencies are close to resonance, these terms can be omitted using the rotating-wave approximation (RWA). In the case of the quantum Rabi model, the RWA simplifies the Hamiltonian to the standard Jaynes–Cummings model<sup>39</sup> (BOX 1). The Jaynes–Cummings model, which has been a workhorse of quantum optics in the WC and SC regimes, conserves  $\hat{N}_{\text{exc}}$  and restricts the resulting light–matter dynamics to 2D Hilbert subspaces<sup>40</sup>. However, the RWA is not justified in the USC

regime, when all terms in the light–matter interaction come into play.

Although the quantum Rabi model does not conserve  $\hat{N}_{\text{exc}}$ , it does conserve the parity  $\hat{P} = \exp(i\pi\hat{N}_{\text{exc}})$ . A generalized quantum Rabi model, which is obtained by replacing the term  $g \hat{X} \hat{\sigma}_x$  by  $g \hat{X} (\hat{\sigma}_x \cos \theta + \hat{\sigma}_z \sin \theta)$  (with a parameter  $\theta \neq 0, \pi$ ) does not conserve even  $\hat{P}$ ; this Hamiltonian features in experiments with superconducting circuits<sup>12,41</sup>. The Jaynes–Cummings model conserves both  $\hat{N}_{\text{exc}}$  and  $\hat{P}$ .

An analytical approach to finding the spectrum of the quantum Rabi model was discovered only in 2011 (REF.<sup>42</sup>), and has since been extended to multiple two-level systems<sup>43,44</sup> and bosonic modes<sup>45</sup>. But it still requires numerical calculations of transcendental (non-analytical) functions. A particular difficulty is to find exceptional eigenvalues of  $\hat{H}_{\text{Rabi}}$  with no definite parity (doubly degenerate)<sup>42</sup>. In contrast to the quantum Rabi model, the spectrum of the Jaynes–Cummings model is simple and well known<sup>40</sup>.

The quantum Rabi model can be simulated with the standard Jaynes–Cummings model in experiments

**Box 2 | The diamagnetic term**

The minimal-coupling substitution  $\hat{p} \rightarrow \hat{p} - e\hat{A}$  (where  $\hat{p}$  is the momentum,  $e$  is the elementary charge and  $\hat{A}$  is the electromagnetic vector potential) in the kinetic Hamiltonian  $\hat{H}_{\text{kin}} = \frac{\hat{p}^2}{2m}$  (where  $m$  is the mass of the charged particle) leads, when expanding the square, to the appearance of two interaction terms. The first

$$\hat{H}_{\text{int}} = -\frac{e\hat{p}\hat{A}}{m} = \sum_n g_{jn} (\hat{a} + \hat{a}^\dagger) \hat{M}_{jn} \quad (\text{B2.1})$$

is of the form considered in BOX 1, describing a dipolar interaction between the photonic cavity mode and the optically active transitions between the initial state  $|j\rangle$  and all final states  $|n\rangle$ , with  $\hat{M}_{jn}$  a generic transition operator,  $g_{jn}$  the light-matter coupling strengths and  $\hat{a}$  and  $\hat{a}^\dagger$  the annihilation and creation operators of the cavity mode. The second term

$$\hat{H}_{\text{dia}} = \frac{e^2 \hat{A}^2}{2m} = D(\hat{a} + \hat{a}^\dagger)^2 \quad (\text{B2.2})$$

is the one responsible for the appearance of diamagnetism and, being of second order in the electrical charge, is usually of limited importance when studying dipolar transitions outside the ultrastrong-coupling (USC) regime. Of the two interaction terms, only  $\hat{H}_{\text{int}}$  depends on the mode structure of the matter degrees of freedom. Using a few-level description of the matter part can thus lead to an overestimation of the diamagnetic term compared with the approximated  $\hat{p}\hat{A}$  term. The Thomas–Reiche–Kuhn sum rule,  $\sum_n \frac{|(n|\hat{p}|j)|^2}{\omega_{jn}} = \frac{m}{2}$ , with  $\omega_{jn}$  the frequency of the  $|j\rangle \rightarrow |n\rangle$  transition, can then be used to establish a minimum value of  $D$  for the considered model. To do so, we start by rewriting  $\hat{H}_{\text{dia}}$  as

$$\hat{H}_{\text{dia}} = \left( \sum_n \frac{|(n|\hat{p}|j)|^2}{\omega_{jn}} \right) \frac{e^2 \hat{A}^2}{m^2} = \sum_n \frac{g_{jn}^2}{\omega_{jn}} (\hat{a} + \hat{a}^\dagger)^2 \quad (\text{B2.3})$$

Comparing equations B2.2 and B2.3, we can read  $D = \sum_n \frac{g_{jn}^2}{\omega_{jn}}$ , implying that, when any single quasi-resonant transition of frequency  $\omega_x$  and coupling  $g$  is considered

$$D \geq \frac{g^2}{\omega_x} = g\eta \quad (\text{B2.4})$$

The ratio of the coefficients of the diamagnetic and dipolar parts of the light-matter interaction,  $D/g$ , is thus at least as large as the normalized coupling  $\eta$ , with the equality in equation B2.4 if a single transition saturates the sum rule. The impact of the diamagnetic term is thus non-negligible in the USC regime, and eventually becomes dominant in the deep-strong-coupling regime.

using various tricks, as discussed below. Also, the coupling  $g$  can be enhanced in various ways, for example, by increasing the number of two-level systems or cavity fields, or by applying classical (single-photon) drives to a single two-level system or a cavity field. Recently, an exponential enhancement of  $g$  was predicted with a two-photon drive (squeezing) of the cavity field<sup>46,47</sup>.

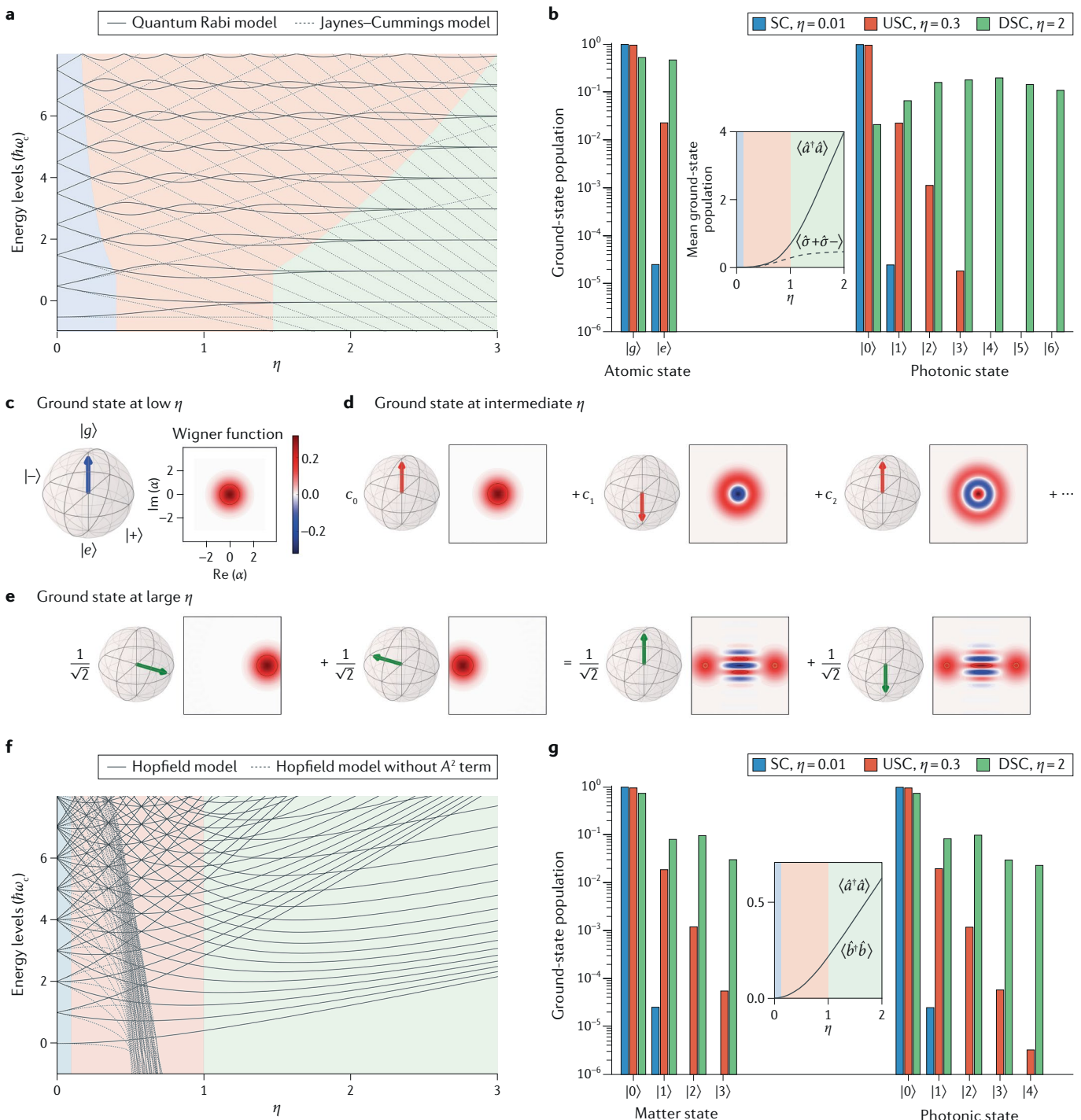
A generalization of the quantum Rabi model to  $N$  two-level systems (which can correspond to a single multi-level system or a large spin) is known as the Dicke model<sup>8</sup>. Under the RWA, the Dicke model reduces to the Tavis–Cummings model<sup>48</sup> (BOX 1). Another generalized version of the quantum Rabi model, with  $g_1 \neq g_2$ , enables the study of supersymmetry (SUSY), which exists if  $g_1^2 - g_2^2 = \omega_e \omega_q$  (that is, when the Bloch–Siegert shift is zero)<sup>50</sup>. Note that  $g_1 = g_2$  if the Rabi model is derived from first principles.

The Hamiltonian for the Hopfield model is given in BOX 1. In this case, the  $g_i$  terms describe parametric frequency conversion, which conserves the total number of excitations  $\hat{N}_{\text{exc}}$ , while the  $g_2$  terms describe parametric amplification, which does not conserve  $\hat{N}_{\text{exc}}$ . These processes, often studied in quantum optics, are analogous to those described by  $\hat{H}_{\text{int}}$  for the quantum Rabi model.

This simplified Hopfield model has been applied to describe experimental data of a 2D electron gas interacting with terahertz cavity photons in the USC regime<sup>51–53</sup>.

**Other regimes of light-matter coupling.** For the sake of completeness, we mention here three other regimes of light-matter coupling. The first is the deep-strong-coupling (DSC, FIG. 1f) regime, in which  $\eta$  becomes larger than 1 and higher-order perturbative processes are not only observable but can become dominant. Theoretically investigated for the first time in 2010 (REF.<sup>54</sup>), this regime was finally demonstrated experimentally in 2017 using different physical implementations<sup>21,41</sup>.

The second, the very-strong-coupling (VSC) regime, is achieved when  $g$  becomes comparable to the spacing between the excited levels of the quantum emitter. In this regime, although the number of excitations is conserved and first-order perturbation gives an adequate description of the system, the coupling is large enough to hybridize different excited states of the emitter, modifying its properties. This regime was initially predicted by Khurgin in 2001 (REF.<sup>55</sup>), and observed in microcavity polaritons in 2017 (REF.<sup>56</sup>).



The third is the multi-mode-strong-coupling (MMSC) regime, in which  $g$  exceeds the free spectral range of the resonator that the matter couples to. This regime has recently been reached with superconducting qubits coupled to either microwave photons in a long transmission-line resonator<sup>31</sup> or phonons in a surface-acoustic-wave resonator<sup>57</sup>.

In the rest of this Review, we largely speak of USC, with the implicit understanding that, according to the value of  $\eta$  and other energy scales, the system under investigation could also be in the WC, SC, VSC, MMSC or DSC regimes.

### Properties of systems with USC

As  $\eta$  increases, several properties of coupled light-matter systems change drastically. The lowest energy levels of a light-matter system with a single atom on resonance with a cavity mode as a function of  $\eta$  are plotted in FIG. 2a. Only the quantum Rabi model (BOX 1) gives a correct picture of the energy levels for all  $\eta$ ; various approximate methods can be used for small or large  $\eta$ . The Jaynes–Cummings model correctly predicts the Rabi splitting (dressed states) between neighbouring pairs of energy levels, but fails when the system enters the USC regime.

**Fig. 2 | Spectrum and ground-state properties of ultrastrongly coupled light–matter systems.** **a** | The lowest energy levels (offset by  $+hg^2/\omega_c$ ) of the quantum Rabi Hamiltonian as a function of the normalized coupling strength  $\eta$ . For comparison, the same levels for the Jaynes–Cummings Hamiltonian are also plotted. The two models coincide in the shaded blue area, in which perturbation theory using  $\eta$  as a small parameter works well. The cross-over into the shaded red area, in which perturbation theory no longer works, takes place around the Juddian points, in which pairs of energy levels begin to cross. Once  $\eta$  is well past 1 (shaded green area), other parameters become comparatively small and can be used for perturbative expansions. The cross-over to this regime is marked by pairs of energy levels starting to become degenerate<sup>16,218</sup>. More details can be found in REF.<sup>219</sup> **b** | Representative ground-state statistics for the strong-coupling (SC), ultra-strong-coupling (USC), and deep-strong-coupling (DSC) regimes of the quantum Rabi model. We apply the usual convention in which USC encompasses  $0.1 < \eta < 1$ . As the coupling increases, the ground state of the quantum Rabi model starts to contain a considerable number of (virtual) atomic and photonic excitations. **c** | The ground state of the quantum Rabi model for low coupling strength is well approximated as  $|E_0\rangle \approx |g\rangle|0\rangle$ , here illustrated with a Bloch sphere representation for the atomic state and a Wigner-function representation for the photonic state. **d** | In the non-perturbative USC regime, no simple expression for the ground state of the quantum Rabi model exists. It is a superposition of all states with an even number of excitations:  $|E_0\rangle = c_0|g\rangle|0\rangle + c_1|e\rangle|1\rangle + c_2|g\rangle|2\rangle + c_3|e\rangle|3\rangle + \dots$  where, as can be seen in part **b**,  $|c_0|^2 > |c_1|^2 > \dots$  **e** | As the coupling is increased further into the perturbative DSC regime, the ground state of the quantum Rabi model can be approximated well as  $|E_0\rangle \approx (|+\rangle|\alpha\rangle + |-\rangle|-\alpha\rangle)/\sqrt{2}$ , where  $|\pm\rangle = (|g\rangle \pm |e\rangle)/\sqrt{2}$  are the eigenstates of  $\hat{\sigma}_x$  and  $|\alpha\rangle$  is the coherent state with  $\alpha = \sqrt{\langle \hat{a}^\dagger \hat{a} \rangle}$ . An interesting feature of this ground state is that it can be rewritten as  $(|g\rangle(|\alpha\rangle - |\-\alpha\rangle) + |e\rangle(|\alpha\rangle + |\-\alpha\rangle))/\sqrt{2}$  up to a normalization factor, which means that the atom is entangled with photonic Schrödinger’s cat states. **f** | Same as panel **a**, but for the Hopfield model with and without the  $A^2$  term. For the latter case, the sharp drop-off beginning at  $\eta = 0.5$  marks the superradiant phase transition. **g** | Same as part **b**, but for the Hopfield model.  $\hbar$ , reduced Planck’s constant;  $g$ , strength of light–matter coupling;  $\omega_c$ , frequency of the cavity mode;  $\hat{a}$  and  $\hat{a}^\dagger$  annihilation and creation operators for the cavity mode, respectively;  $\hat{\sigma}_x$ , Pauli operator. Panel **a** is adapted with permission from REF.<sup>219</sup>, APS.

**Ground-state properties.** The difference between the USC and non-USC regimes is particularly striking for the ground state of a coupled light–matter system (FIG. 2b–e). For small  $\eta$ , the lowest energy state of the system is simply an empty cavity with the atom in its ground state. However, as  $\eta$  grows the coupling makes it increasingly energetically favourable to have atomic and photonic excitations in the ground state. The exact nature of these excitations is discussed in the section on virtual excitations. Here we only note that for very large  $\eta$ , in the DSC regime (FIG. 2e), the ground state of the quantum Rabi model consists of photonic Schrödinger’s cat states entangled with the atom and exhibits non-classical properties such as squeezing<sup>16,58</sup>.

The mean number of photons in the ground state starts to increase rapidly when the value of  $\eta$  approaches and passes 1 (FIG. 2b). In the case of many atoms coupled to the light, as described by the Dicke model (BOX 1), it is predicted that a quantum phase transition, known as the superradiant phase transition<sup>59–61</sup>, takes place at a critical value of  $\eta$ , separating phases with and without photons in the ground state of the system. However, as explained below, whether or not this phase transition actually occurs depends on whether an additional term, the diamagnetic term, should be included in the Hamiltonian. Furthermore, the recent realization of USC in systems with artificial atoms raises the question of whether the superradiant phase transition occurs when the transition

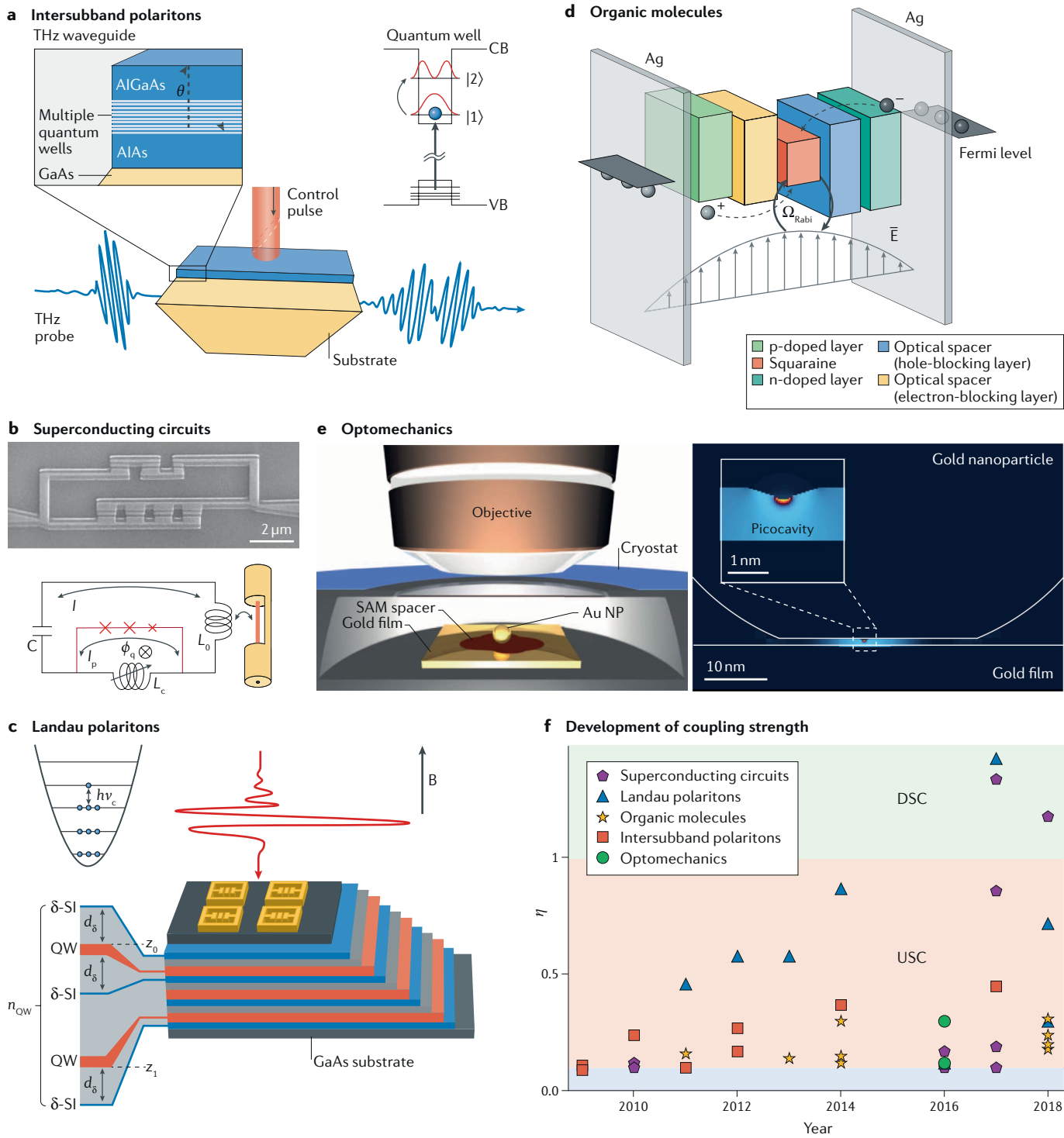
frequencies and coupling strengths of individual atoms differ<sup>62</sup>. We also note that several works, such as REF.<sup>63</sup>, have analysed the physics at the critical value of  $\eta$  in the quantum Rabi model instead, in which the thermodynamic limit of infinitely many atoms cannot be realized.

In FIG. 2f we plot the energy levels for the case in which the matter instead consists of many atoms and is described as bosonic collective excitations in the Hopfield model (BOX 1). The impact of the diamagnetic term is clearly seen. FIGURE 2g shows the ground-state population with the diamagnetic term included. Also in this case, the ground state contains virtual light and matter excitations. This ground state can be calculated analytically<sup>64</sup> for all  $\eta$ ; it is a multi-mode squeezed state for large  $\eta$ .

**The diamagnetic term.** In the DSC regime, the diamagnetic term (BOX 2) can act as a potential barrier for the photonic field, localizing it away from the dipoles, leading to an effective decoupling between the light and matter degrees of freedom<sup>30</sup>. This means that the Purcell effect, known from the WC regime and thought to increase the rate of spontaneous emission of the qubit with increasing  $g$ , actually becomes negligible when  $g$  becomes large enough. A similar decoupling can occur if qubit–qubit interactions are added to the Dicke model<sup>65</sup>. Even in the pure quantum Rabi model, unexpected changes in photon output statistics take place deep in the DSC regime<sup>66</sup>.

Being a consequence of gauge invariance, the diamagnetic term is required to obtain a consistent theory, including in superconducting systems. Claims have been advanced on the possibility of engineering systems, both dielectric<sup>67</sup> and superconducting<sup>68</sup>, in which the diamagnetic term is absent or at least reduced to violate equation B2.4. Those claims have attracted strong criticism<sup>69,70</sup>. There have also been theoretical proposals showing how the matter could be experimentally settled<sup>71–73</sup>.

This interest in the presence of the diamagnetic term in cavity QED is historically due to its supposed role in stabilizing a system against the occurrence of superradiant phase transitions. It is easy to gain an intuitive understanding of why such a term could stabilize the ground state of the system. The diamagnetic term can be removed from the Hamiltonian by performing a Bogoliubov rotation in the space of the photon operator, at the cost of a renormalization of the cavity frequency:  $\omega_c \rightarrow \sqrt{\omega_c^2 + 4\omega_c D}$ , where  $D$ , discussed in BOX 2, is a measure of the energy of the diamagnetic term. For the system to undergo a quantum phase transition, the coupling has to be strong enough to push one of the system eigenmodes to zero frequency. The blueshift of the cavity due to the renormalization thus implies that a larger coupling  $g$  is required to reach the critical point, but from equation B2.4 this in turn will further blueshift the cavity mode. A careful calculation shows that, at least for the Dicke model, this runaway process leads to a divergent critical value of  $g$  if equation B2.4 holds. Notwithstanding this simple argument, a number of works have reported opposite views on the possibility of achieving superradiant phase transitions<sup>36,69,74–81</sup>.



These seemingly contrasting arguments are presently understood to be at least partially due to the role of long-range dipole–dipole interactions, which depend on the specific geometry of the system under consideration and can lead to very different results owing to the choice of gauge and of dynamical variables<sup>37,76,81</sup>.

The presence in the Hamiltonian of an  $A^2$  term is not gauge invariant. For example, in the Power–Zienau–Woolley form of the Hamiltonian, in which matter is

described by a polarization density  $P$ , there is no  $A^2$  term, but a  $P^2$  term is present, quadratic in the matter instead of in the photonic field<sup>77,82</sup>. Finally, it is worth noting that the presence of a squared field term in the Hamiltonian, which assures the stability of matter linearly coupled to a bosonic field, is a feature that is not limited to the interaction with the transverse electromagnetic field. Similar terms, satisfying the equivalent of equation B2.4, have been derived in the case of longitudinal interactions in intersubband polaritons<sup>83</sup>.

◀ Fig. 3 | **Experimental systems with ultrastrong light-matter coupling.**

**a** | Intersubband polaritons. In REF.<sup>87</sup>, a transition between subbands |1⟩ and |2⟩ in the conductance band (CB) of multiple quantum wells (MQWs) was activated by a near-infrared control pulse exciting electrons from the valence band (VB). The intersubband transition coupled to transverse-magnetic-polarized cavity photons propagating at an angle  $\theta$ , resulting in a coupling strength  $\eta = 0.09$ .

**b** | Superconducting circuits. In REF.<sup>41</sup>, a flux qubit consisting of three Josephson junctions in a loop (image and red part of the diagram) coupled inductively to a lumped-element LC circuit, reaching  $\eta = 1.34$ .

**c** | Landau polaritons. In REF.<sup>21</sup>, a stack of quantum wells hosting 2D electron gases with Landau levels (set by an external magnetic field  $B$ ) separated by the cyclotron frequency  $v_c$ , were coupled to an array of THz resonators on top of the stack, reaching  $\eta = 1.43$ .

**d** | Organic molecules. In REF.<sup>14</sup>, squaraine dye was placed between layers of organic materials (p- and n-doped layers and optical spacers) in a microcavity formed by Ag mirrors, forming an organic light-emitting diode reaching  $\eta = 0.3$ .

**e** | Optomechanics. The vibrational modes of biphenyl-4-thiol molecules in a self-assembled monolayer (SAM) interact with light localized in a ‘picocavity’ formed between a gold film and a single gold atom on the surface of a gold nanoparticle, reaching  $\eta = 0.3$  (REF.<sup>117</sup>).

**f** | Measured  $\eta$  for all experiments that have achieved ultrastrong coupling (USC), excluding experiments with USC to a continuum and quantum simulations of USC.

In something that can be called Moore’s law for light–matter coupling strength, the past decade has seen experiments progressing steadily from breaking the barrier to the USC regime to entering the deep-strong-coupling (DSC) regime.  $E$ , electric field. Panel **a** is reproduced with permission from REF.<sup>117</sup>, AAAS. Panel **b** is reproduced from REF.<sup>41</sup>, Springer Nature Limited. Panel **c** is reproduced with permission from REF.<sup>14</sup>, ACS. Panel **d** is reproduced from REF.<sup>87</sup>, Springer Nature Limited. Panel **e** is reproduced with permission from REF.<sup>21</sup>, ACS.

### Experimental systems with USC

The first experimental demonstration of ultrastrong ( $\eta > 0.1$ ) light–matter coupling was reported in 2009 (REF.<sup>11</sup>). USC has since been achieved in several different systems and at different wavelengths (FIG. 3). In 2017, two experiments even managed to reach DSC ( $\eta > 1$ )<sup>21,41</sup>. The past decade has seen a rapid increase in values of  $\eta$  (FIG. 3f; TABLE 1). However, it should be noted that fitting experimental data to theoretical models to extract  $\eta$  can be a subtle and demanding task in the USC and DSC regimes<sup>35</sup>.

**Intersubband polaritons.** The USC regime was first predicted<sup>10</sup> and demonstrated<sup>11</sup> exploiting intersubband polaritons in microcavity-embedded doped quantum wells (FIG. 3a). In these systems, nanoscopic layers of different semiconductors create a confining potential for carriers along the growth direction, which splits electronic bands into discrete parallel subbands. Thanks to the quasi-parallel in-plane dispersion of the different conduction subbands, all the electrons in the conduction band can be coherently excited, creating narrow collective optical resonances. The coupling of these resonances with transverse-magnetic polarized radiation scales with the square root of the total electron density. By modifying the width of the quantum wells, the resonances can be tuned to cover the THz and mid-infrared sections of the electromagnetic spectrum.

Intersubband-polariton systems are usually well described by the Dicke model. This was exploited in REF.<sup>11</sup>, in which a demonstration of USC with  $\eta = 0.11$  was obtained by comparing experimental data with best fittings obtained using the Dicke model with and without anti-resonant terms.

However, this appealingly simple model is not appropriate for more complex devices. The presence of multiple quasi-resonant photonic modes can lead to a

physics described by the quantum Rabi model instead<sup>84</sup>. Moreover, as the width of the quantum wells increases and multiple electron transitions become available, the intuitive picture in terms of single-particle states is lost. In that case, the electronic transition is better described as a plasma-like mode<sup>85,86</sup>.

Intersubband polaritons remain a scientifically and technologically interesting system in which to study USC phenomenology thanks to the possibility of non-adiabatically modifying the coupling strength<sup>87</sup>, which makes it a promising platform for quantum vacuum emission experiments<sup>88,89</sup>. Moreover,  $\eta$  has been progressively increased in various experiments<sup>85,90–93</sup> up to the present value of  $\eta = 0.45$  (REF.<sup>86</sup>).

**Superconducting circuits.** The next experiments to reach USC, in 2010 (REF.<sup>12,13</sup>), used superconducting quantum circuits. In these systems, electrical circuits with Josephson junctions, operating at GHz frequencies, function as ‘artificial atoms’, acquiring a level structure similar to that of natural atoms when cooled to millikelvin temperatures. These artificial atoms are then coupled to photons in resonators formed by an inductance  $L$  and a capacitance  $C$  in a lumped-element circuit or in a transmission line. Superconducting circuits are a powerful platform for exploring atomic physics and quantum optics and for QIP, because their properties (such as the resonance frequencies and coupling strength) can be designed and even tuned *in situ*<sup>7</sup>. This has been widely exploited in the SC regime, for example, to engineer quantum states and realize quantum gates.

The superconducting quantum circuit experiments<sup>12,13,33,41,94–98</sup> are the only ones that have achieved USC with a single (albeit artificial) atom. The reason why superconducting circuits, unlike other systems, do not require collective excitations to reach USC, is that the coupling scales differently with  $\alpha$  in these circuits<sup>9</sup>. In cavity QED, the coupling scales as  $\alpha^{3/2}$ . In circuit QED, it scales as either  $\alpha^{1/2}$  or  $\alpha^{-1/2}$ , depending on the layout of the superconducting circuit<sup>9</sup>.

The design of the first system to break the DSC barrier<sup>41</sup> (with  $\eta = 1.34$ ) is shown in FIG. 3b. As discussed in more detail below, superconducting quantum circuits are also the only systems in which USC to a continuum<sup>99–101</sup> has been demonstrated, and they have proven to be an excellent platform for quantum simulation of USC<sup>102,103</sup>.

**Landau polaritons.** Since 2011, the record for  $\eta$  has almost continuously been held by Landau-polariton systems. In these systems, based on microcavity-embedded doped quantum wells under a transverse magnetic field, the USC occurs between a photonic resonator and the collective electronic transitions between continuous Landau levels. In contrast with intersubband polaritons, whose dipole lies along the growth axis, Landau transitions have an in-plane dipole and thus couple to transverse electrical-polarized radiation. The very large coupling achievable in these systems is due to an interplay between the degeneracy of Landau levels, the transition dipole, which increases with the index of the highest occupied Landau level, and the relatively small cyclotron frequencies in the THz or GHz range observable in high-mobility heterostructures.

Table 1 | Experiments that have achieved ultrastrong light–matter coupling

	Year	$\eta$	Reference
<b>Intersubband polaritons</b>	2009	0.11	11
	2009	0.09	87
	2010	0.24	90
	2011	0.10	91
	2012	0.27	92
	2012	0.17	93
	2014	0.37	85
	2017	0.45 <sup>a</sup>	86
<b>Superconducting circuits</b>	2010	0.12	12
	2010	0.10	13
	2016	0.10	94
	2016	0.17	95
	2017	0.19	33
	2017	0.10	96
	2017	1.34 <sup>a</sup>	41
	2017	0.86	97
	2018	1.18	98
<b>Landau polaritons</b>	2011	0.46	108
	2012	0.58	104
	2013	0.58	105
	2014	0.87	106
	2016	0.12	52
	2017	1.43 <sup>a</sup>	21
	2018	0.72	107
	2018	0.30	109
<b>Organic molecules</b>	2011	0.16	111
	2013	0.14	112
	2014	0.30	14
	2014	0.12	113
	2014	0.15	114
	2018	0.31 <sup>a</sup>	115
	2018	0.18	110
	2018	0.20	15
<b>Optomechanics</b>	2018	0.24	116
	2016	0.12	32
	2016	0.30 <sup>a</sup>	117

The data in this table are plotted in FIG. 3f. <sup>a</sup>The highest normalized coupling strength  $\eta$  achieved for each experimental system.

Theoretically described for the first time in 2010 (REF.<sup>51</sup>), Landau-polariton systems with USC were observed shortly afterwards using split-ring resonators<sup>21,104–107</sup> (FIG. 3c), photonic-crystal cavities<sup>52,53</sup> and coplanar microresonators<sup>108</sup>. The present record value of light–matter coupling,  $\eta = 1.43$ , was measured in REF.<sup>21</sup>.

Landau-polariton systems are a useful platform for investigating USC phenomenology. In REF.<sup>53</sup>, the polarization selectivity of the Landau transition was used to directly measure the Bloch–Siegert shift due to the anti-resonant terms in the Hamiltonian. Furthermore, in REF.<sup>109</sup>, magnetotransport was used to investigate the

nature of the matter excitations participating in the Landau-polariton formation. In REF.<sup>21</sup>, light–matter decoupling in the DSC regime was reported for the first time, and also exploited to optimize the design of the photonic resonator.

**Organic molecules.** The USC regime has also been realized at room temperature at a variety of optical frequencies coupling cavity photons (or, in one case, plasmons<sup>110</sup>) to Frenkel molecular excitons<sup>14,15,111–116</sup>. These systems consist of thin films of organic molecules with giant dipole moments (which make it possible

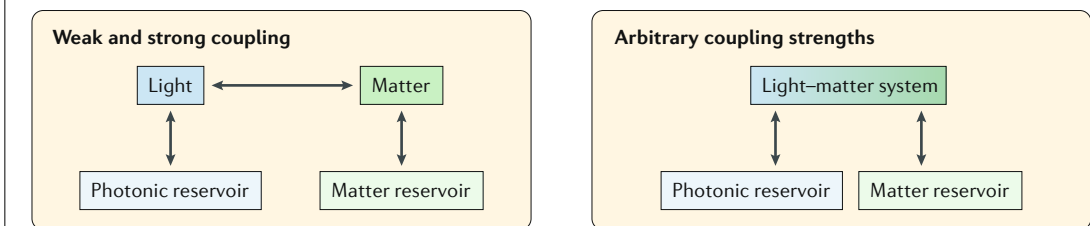
**Box 3 | Treating open quantum systems in the USC regime**

No quantum system is completely isolated from its environment. Control and readout imply a coupling with the outside world, leading to dissipation and decoherence. Textbook quantum-optical procedures to treat open quantum systems neglect the interaction between their constituent subsystems when describing their coupling to the environment<sup>223</sup>. This results in a set of dynamical equations in which each subsystem couples to the environment at its own bare frequency. This white-reservoir approximation fails dramatically in the ultrastrong-coupling (USC) regime, as it does not take into account that the environment density of states vanishes at negative frequencies. The large frequency shifts of the USC regime in fact push part of the system's spectral weight to negative frequencies. A frequency-independent environment density of states thus allows for coupling the system with negative-frequency modes, making the ground state unstable even at zero temperature.

This problem was solved in REF.<sup>129</sup> by using a master equation with coloured reservoirs. A general approach to project the master equation onto the coupled eigenbasis was then developed in REF.<sup>119</sup> and it has been the subject of various other works<sup>16,120,121,224–226</sup>. Numerical simulation of the resulting master equations can become computationally demanding for larger values of the coupling strength  $\eta$ , because the increasing number of virtual photons requires exponentially larger simulation cutoffs.

A method both analytically simpler and numerically lighter is the bosonic input–output theory, in which the system dynamics is integrated out to derive the scattering matrix. This approach was initially introduced for the USC regime in REF.<sup>124</sup> and further developed in subsequent work<sup>224,227,228</sup>. Although applicable only to bosonic quadratic Hamiltonians, this approach has the advantage of being non-perturbative. It thus enables investigation of loss-dominated regimes, for example, allowing study of impact of the environment on the population of ground-state virtual excitations<sup>29</sup>.

The figure shows how, as the light–matter coupling strength increases, it becomes necessary to describe the interaction with the environment in terms of the coupled eigenmodes of the light–matter system.



to reach USC) sandwiched between metallic mirrors (FIG. 3d) and present an interesting combination of high coupling strengths and functional capacities. A vacuum Rabi splitting beyond 1 eV, corresponding to  $\eta=0.3$ , has been reported<sup>14,115</sup>. Using such high coupling strengths, monolithic organic light-emitting diodes working in the USC regime have been fabricated<sup>14,15,113,114,116</sup>. These devices exhibit a room temperature dispersion-less angle-resolved electroluminescence with very narrow emission lines that can be exploited to realize innovative optoelectronic devices.

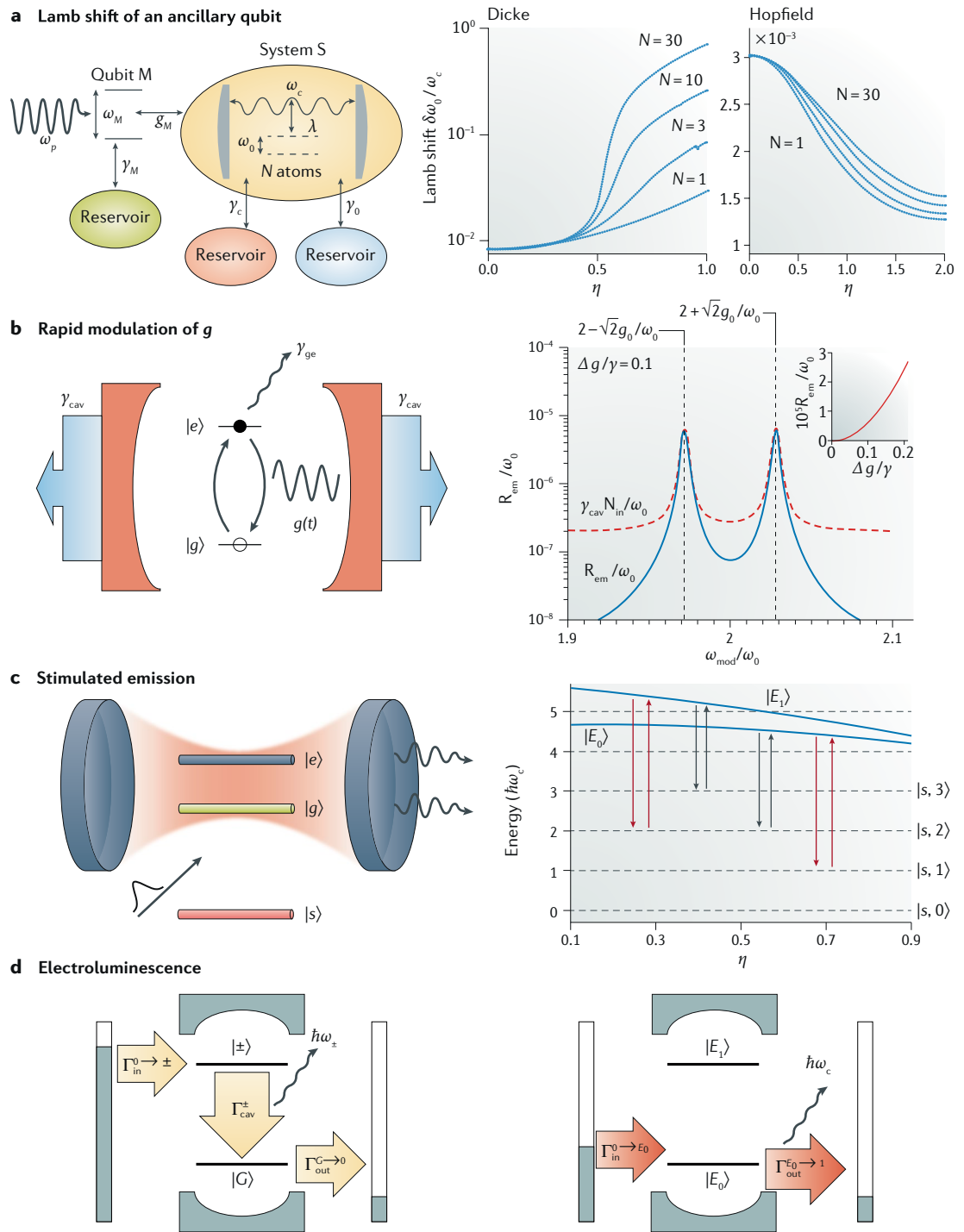
**Optomechanics.** The concept of ultrastrong light–matter interaction can be extended to optomechanics. Recently, the USC limit was reached in a setup in which plasmonic picocavities interacted with the vibrational degrees of freedom of individual molecules<sup>117</sup> (FIG. 3e), achieving  $\eta=g/\omega_m=0.3$  ( $\omega_m$  is the mechanical frequency). The increase in coupling strength is due to the small mode volume of the picocavity, which circumvents the diffraction limit to confine optical light in a volume of a few cubic nanometers.

Another approach to increase the optomechanical coupling strength is to use molecules with high vibrational dipolar strength. This was the approach used in REF.<sup>32</sup>, in which  $\eta=0.12$  was reached. The USC limit has also been approached in circuit-optomechanical systems by using the nonlinearity of a Josephson-junction qubit to boost  $\eta$ <sup>118</sup>.

### Virtual excitations

A clear difference between USC systems and systems with lower coupling strength is the presence of light and matter excitations in the ground state (FIG. 2). This difference is due to the influence of the counter-rotating terms in the Hamiltonian (BOX 1). At lower coupling strength, excited states of the system can be ‘dressed states’, superpositions of two states containing both light and matter excitations<sup>40</sup>. These two states contain the same number of excitations. However, in the USC regime, all excited states are dressed by multiple states containing different numbers of excitations. Much research on USC systems has dealt with understanding whether these excitations dressing the system states (especially the ground state) are real or virtual, how they can be probed or extracted, how they make possible higher-order processes that mirror nonlinear optics<sup>20</sup> (see also the section on applications) and how they affect the description of input and output for the system (BOX 3).

**Dressed states and input–output theory.** A correct treatment of input–output, decoherence and correlation functions for a USC system requires taking into account that the system operators coupling it to the outside world no longer induce transitions between the bare states of the system (which have fixed numbers of photons and atomic excitations). Instead, the transitions are between the dressed, true eigenstates of the system



(which contain contributions from various numbers of photons and atomic excitations)<sup>16,119–121</sup>. Following the development of such a treatment, several interesting properties of USC systems have been revealed. For example, whereas thermal emission of photons is supposed to be bunched (photons tend to be emitted together) and photon emission from a single atom is supposed to be anti-bunched (photons are emitted one by one), the photons emitted from a thermalized cavity in the USC regime can be anti-bunched<sup>122</sup> and a two-level atom coupled ultra-strongly to a cavity can emit bunched photons<sup>123</sup>.

A simple way to understand the issue of open quantum systems in the USC regime is to remember that because the Hamiltonian of such a system is non-number conserving, its ground state contains a finite population of virtual excitations (FIG. 2). Assuming that the emitted radiation is just proportional to the photon population in the cavity, neglecting to discriminate between real and virtual particles leads to the prediction of unphysical radiation from the ground state<sup>120,124</sup>. As first shown for confined polaritons<sup>125</sup>, the quantum operators that correctly describe the emission of an output photon in the USC regime contain contributions

**◀ Fig. 4 | Proposed methods for probing and extracting virtual photons dressing the states of an ultrastrongly coupled system.** **a** | To probe the ground state of a system S ( $N$  atoms with frequencies  $\omega_0$ , coupled with strength  $\lambda$  to a cavity mode with frequency  $\omega_c$ ) described by the quantum Rabi, Dicke or Hopfield models (BOX 1), one option is to connect an ancillary qubit M (transition frequency  $\omega_M$ ) to the cavity<sup>127</sup>, as sketched on the left ( $\gamma$  are relaxation rates). The coupling  $g_M$  is not ultrastrong. The right panel shows how, for the Dicke and Hopfield models, the Lamb shift of the qubit M depends on  $N$  and on the coupling strength  $\eta$ . One way to read out this shift is to send in a probe tone at a frequency  $\omega_p$  and monitor the population of the qubit M. Note that the qubit cannot absorb any ground-state photons from the system, because they are bound<sup>126</sup>. **b** | Virtual photons in the ground state of an ultrastrongly coupled system can be released by modulating the coupling  $g(t)$  around its original value  $g_0$  at a frequency  $\omega_{\text{mod}}$  with an amplitude  $\Delta g$  (left panel)<sup>129</sup>. The photon emission rate  $R_{\text{em}}$  (right panel, blue curve) has two peaks close to  $\omega_{\text{mod}} = 2\omega_0$  ( $\omega_0$  denotes the cavity and qubit frequencies). The inset shows the emission rate at one of the peaks as a function of  $\Delta g$  (scaled by the relaxation rates  $\gamma$ ). Note that this calculation requires the proper treatment of input–output theory for ultrastrong coupling (USC; BOX 3). The red curve is the prediction from the standard theory; this predicts unphysical photon emission at all modulation frequencies, proportional to the number of intracavity photons,  $N_{\text{in}}$ . **c** | Virtual photons can also be extracted from an USC system through stimulated transitions. The left panel depicts a three-level atom with its upper transition ( $|g\rangle \leftrightarrow |e\rangle$ ) coupled ultrastrongly to a cavity mode. The solid curves in the right panel show the first and second energy levels for the ultrastrongly coupled part of this system. However, because the transitions  $|s\rangle \leftrightarrow |g\rangle$  and  $|s\rangle \leftrightarrow |e\rangle$  are not ultrastrongly coupled to the cavity, there may be states  $|s, n\rangle$  (atom in  $|s\rangle$  and  $n$  photons in the cavity) that have lower energy. Stimulating a transition  $|s\rangle \leftrightarrow |g\rangle$  (red arrows) or  $|s\rangle \leftrightarrow |e\rangle$  (grey arrows) can thus release or absorb  $n$  photons in the cavity<sup>143</sup>. **d** | Another way to stimulate the release of photons from a USC ground state is electroluminescence. In standard electroluminescence (left panel), a current flowing at a rate  $\Gamma$  from the reservoir on the left through an electronic two-level system coupled to a photonic cavity can release a photon if the electron occupies an excited state  $|\pm\rangle$  and then relaxes to the ground state  $|G\rangle$  before passing to the reservoir on the right. However, as shown in the right panel, the presence of virtual photons in the USC ground state  $|E_0\rangle$  allows a current passing only through  $|E_0\rangle$  to release photons (the required energy is provided by the energy difference between the reservoirs)<sup>19</sup>. Panel **a** is reproduced with permission from REF.<sup>127</sup>, APS. Panel **b** is reproduced with permission from REF.<sup>129</sup>, APS. Panel **c** is reproduced from REF.<sup>143</sup>, CC-BY-3.0. Panel **d** is adapted with permission from REF.<sup>19</sup>, APS.

from both bare annihilation and bare creation cavity-photon operators.

The resulting input–output relation contains the positive-frequency operator  $\hat{X}^+ = \sum_{i < j} X_{ij} |E_i\rangle \langle E_j|$  instead of the cavity-mode annihilation operator  $a$ <sup>120</sup>. Here,  $|E_i\rangle$  are the dressed eigenstates of the USC system, ordered such that  $E_j > E_i$  for  $j > i$ . The coefficients  $X_{ij}$  are matrix elements between eigenstates. In the simplest case  $X_{ij} = \langle E_i | \hat{a} + \hat{a}^\dagger | E_j \rangle$ . The operator  $\hat{X}^+$  can be interpreted as the operator describing the annihilation of physical photons in the interacting system. Analogously,  $\hat{X}^- \equiv (\hat{X}^+)^\dagger$  corresponds to the creation operator. Interestingly, whereas in the ground state  $|E_0\rangle$  of a system in the USC regime the number of bare photons is nonzero,  $\langle E_0 | a^\dagger a | E_0 \rangle \neq 0$  (FIG. 2), the definition of  $\hat{X}^+$  automatically implies that the number of detectable photons is zero:  $\langle E_0 | \hat{X}^- \hat{X}^+ | E_0 \rangle = 0$ .

**Probing and extracting virtual photons.** The photons in the ground state of a system with an atom ultrastrongly coupled to a cavity are not only unable to leave the cavity, they are tightly bound to the atom<sup>35</sup>. The ground-state photons also cannot be detected by a photoabsorber, even if this absorber is placed inside the cavity, except with very small probability at short timescales set by the time–energy uncertainty<sup>126</sup>. In light

of these properties, the ground-state photons in an USC system are considered virtual. However, even though these virtual photons cannot be absorbed by a detector, there are still ways to probe them. One proposal is to measure the change they produce in the Lamb shift of an ancillary probe qubit coupled to the cavity<sup>127</sup> (FIG. 4a); another option is to detect the radiation pressure they give rise to if the cavity is an optomechanical system<sup>128</sup>.

There are also many proposals for how the virtual photons dressing the ultrastrongly coupled ground state  $|E_0\rangle$  (and excited states) can be converted into real ones and extracted from the system. Several of these proposals rely on the rapid modulation of either  $g$  or the atomic frequency<sup>10,88,119,129–135</sup> (FIG. 4b). The generation of photons through the modulation of a system parameter in this way requires USC, but not SC, highlighting that  $g$  is compared with two different parameters in these regimes<sup>29</sup>. A connection can be made between these schemes and the dynamical Casimir effect, in which vacuum fluctuations are converted into pairs of real photons when a mirror (or another boundary condition) is moved at high speed<sup>136–140</sup>.

Another way to extract virtual photons is to use additional atomic levels. If only the upper transition in a Ξ-type three-level atom couples ultrastrongly to the cavity, driving the lower transition can switch that USC on and off<sup>141</sup> to create photons<sup>133</sup>. The virtual photons in the USC part of such a system can also be released through stimulated emission<sup>142</sup>, which opens up interesting prospects for experimental studies of dressed states in the USC regime<sup>143</sup> (FIG. 4c). Finally, if the cavity is ultrastrongly coupled to an electronic two-level system, another way to release photons from  $|E_0\rangle$  is through electroluminescence<sup>19</sup> (FIG. 4d).

### Simulating ultrastrong coupling

Although the USC regime has been reached in several solid-state systems, the experimental effort required to achieve this regime is still considerable. Furthermore, it remains difficult to probe many interesting system properties in these experiments, especially dynamics, for a wide range of parameters. An approach that circumvents these problems is quantum simulation<sup>144,145</sup>, in which an easy-to-control quantum system is used to simulate the properties of the quantum model of interest. In 2010, such an approach was used to observe<sup>146</sup> the superradiant phase transition of the Dicke Hamiltonian by placing a Bose–Einstein condensate in an optical cavity and gradually increasing the effective light–matter coupling through an external pump. Another early example is a classical simulation of the dynamics of the parity chains in the quantum Rabi model, realized in an array of femtosecond-laser-written waveguides in which the waveguide spacing sets the coupling strength and engineered properties of the waveguides set the effective qubit and resonator frequencies<sup>147,148</sup>.

Several proposals for quantum simulation of USC rely on driving some part of a SC system at two frequencies. Then a rotating frame can be found with renormalized parameters, set by the drives, that can be in the USC regime<sup>149–156</sup> (drives can also be used to set effective parameters in other ways<sup>157,158</sup>). In 2017, one such proposal<sup>150</sup>

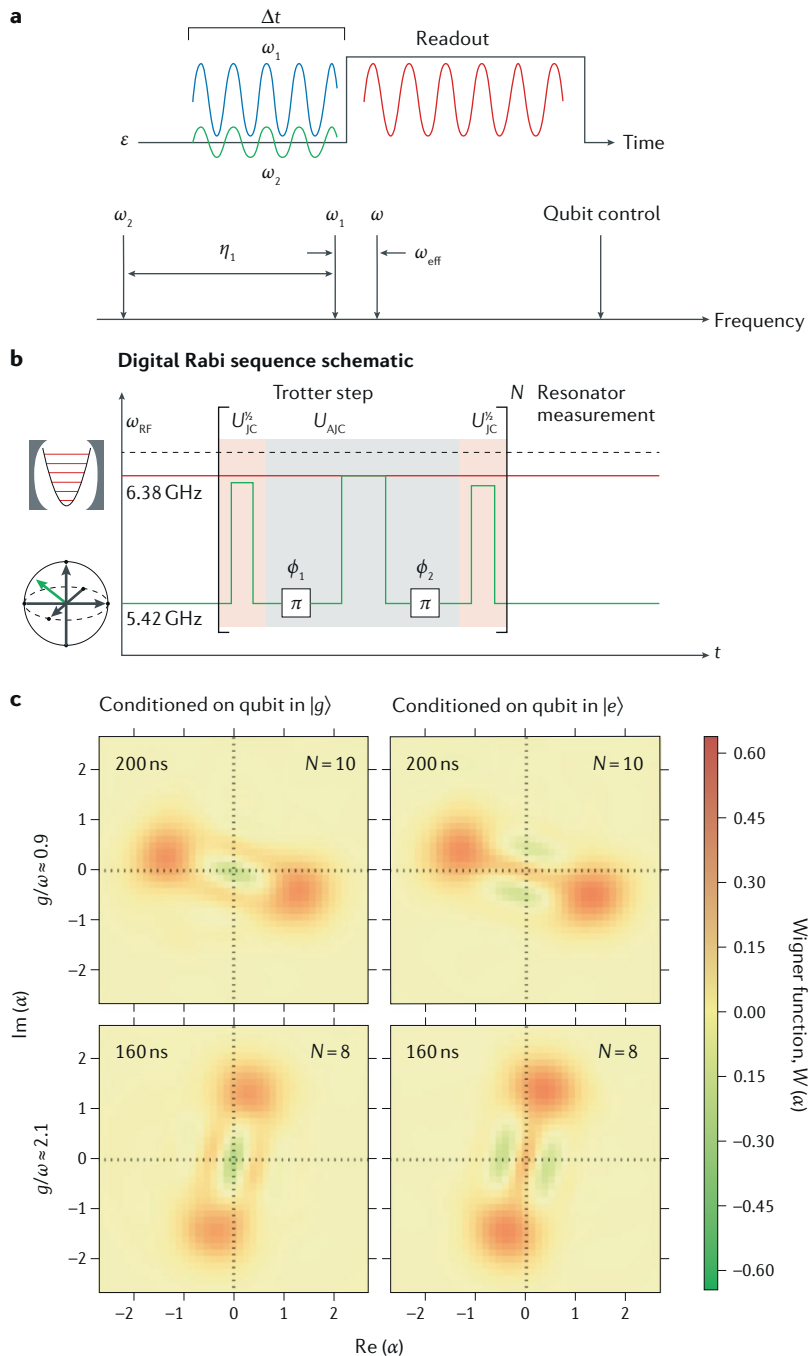


**Fig. 5 | Simulations of ultrastrong coupling.**

**a** | Illustration of the parameters used in the experiment of REF.<sup>103</sup> to simulate ultrastrong coupling (USC) by driving a strongly coupled system with two tones. In the laboratory frame, the qubit has frequency  $\epsilon$  and the resonator has frequency  $\omega$ . Two transversal drives (blue and green curves), with frequencies  $\omega_1$  and  $\omega_2$ , and amplitudes  $\eta_1$  and  $\eta_2$ , respectively, are applied to the qubit. Provided that  $\eta_2 \ll \eta_1 = \omega_1 - \omega_2$ , the Hamiltonian in the interaction picture has an effective qubit frequency  $\epsilon_{\text{eff}} = \eta_2/2$  and an effective resonator frequency  $\omega_{\text{eff}} = \omega - \omega_1$ , but the effective coupling strength is only halved (from originally being  $g$ ):  $g_{\text{eff}} = g/2$ . Even if  $g \ll \epsilon, \omega$ , with the right drive parameters it is possible to simulate  $g_{\text{eff}} \gtrsim \epsilon_{\text{eff}}, \omega_{\text{eff}}$ . After simulating for a time  $\Delta t$ , the qubit is detuned for readout. **b** | Diagram of the digital simulation of USC implemented in the experiment of REF.<sup>102</sup>. Here, the bare resonator frequency is  $\omega_r$  (red line) and the bare qubit frequency is  $\omega_q$  (green line). In one step of the simulation, the qubit is tuned close to the resonator for a short time, detuned and flipped (marked by  $\pi$  and an additional phase shift  $\phi_1$ ), tuned close to resonance again, detuned and flipped (with an additional phase shift  $\phi_2$ ). Due to the two bit flips, the outer interactions with the resonator follow the Jaynes–Cummings Hamiltonian (because the bare coupling  $g \ll \omega_q, \omega_r$ ; BOX 1), whereas the middle interaction follows the anti-Jaynes–Cummings Hamiltonian, that is, the counter-rotating terms. Together, these interactions give the full quantum Rabi Hamiltonian with an effective qubit frequency  $\omega_q^R$  defined by the difference in the detuning of the qubit from the resonator in the different steps, an effective resonator frequency  $\omega_r^R = 2(\omega_r - \omega_{RF})$  ( $\omega_{RF}$  is a frequency defining the rotating frame, set by  $\phi_1 - \phi_2$ ), and an effective coupling strength  $g^R = g$ . After  $N$  repetitions (Trotter steps) of the sequence, the resonator was read out through interaction with another qubit. **c** | Results from simulations of the USC ground state in REF.<sup>102</sup>. The plots show the Wigner functions for the resonator state conditioned on measuring the qubit in its ground state (left column) or excited state (right column) for  $\eta \approx 0.9$  (upper row, 10 Trotter steps) and  $\eta \approx 2.1$  (lower row, 8 Trotter steps). The Schrödinger's cat states emblematic of extremely high coupling strengths (compare with FIG. 2c) are clearly visible. Panel **a** is reproduced from REF.<sup>103</sup>, CC-BY-4.0. Panels **b,c** are reproduced from REF.<sup>102</sup>, CC-BY-4.0.

Jaynes–Cummings model (FIG. 5b). By tuning a qubit in and out of resonance with a resonator, and flipping the qubit inbetween, the quantum Rabi Hamiltonian can be simulated<sup>161,162</sup> (with multiple qubits, this can be straightforwardly extended to simulate the Dicke Hamiltonian<sup>161,162</sup>). This was the approach taken in another recent circuit-QED experiment<sup>102</sup>, which simulated  $\eta$  up to 1.8 and observed dynamics in this regime, including the evolution of the photonic Schrödinger's cat states in the ground state of the quantum Rabi model (FIG. 5c), first predicted in REF.<sup>16</sup>. However, the photons in these simulations are always real, not virtual, like the photons in a physical USC.

### Ultrastrong coupling to a continuum

An atom can couple ultrastrongly not only to a single harmonic oscillator, but also to a collection or continuum of them. This constitutes an interesting and, so

was implemented in a circuit-QED experiment in which two drive tones were applied to a superconducting qubit coupled to a transmission-line resonator<sup>103</sup> (FIG. 5a). Starting from a bare  $\eta < 10^{-3}$ , a simulated  $\eta$  of  $> 0.6$  was achieved and the dynamics of population revivals were observed. Recently, the USC was also simulated in a trapped-ion system<sup>159</sup> using the proposal of REF.<sup>152</sup>, and USC between two resonators was simulated in superconducting circuits<sup>160</sup> following the proposal in REF.<sup>155</sup>.

However, external continuous drives are not necessary to define a rotating frame that places the system in the USC regime. An ingenious digital quantum simulation can be realized with a system described by the

far, less explored regime of the well-known spin-boson model<sup>163,164</sup>. To speak of USC to a continuum, the RWA should not be applicable to the interaction terms in the model, which is an extension of the quantum Rabi model (BOX 1) to many modes. This roughly corresponds to the relaxation rate  $\Gamma$  of the atom into the continuum being 10% or more of the atomic transition frequency  $\omega_q$ . Note that  $\Gamma$  is determined not only by the coupling  $g$  to a single light mode, but also by the density of states  $J(\omega)$  of the continuum. However, if the continuum is modelled as a 1D array of coupled resonators with the atom coupling to one resonator (FIG. 6a), the  $\eta$  from the single-mode case can still be used to define USC.

After USC to a cavity was first realized a decade ago, several theory proposals showed that superconducting circuits were a suitable platform for USC to a continuum (in this case, an open waveguide on a chip)<sup>165–167</sup>. In 2017, such an experiment succeeded<sup>168</sup> (FIG. 6b) and more demonstrations have followed<sup>100,101</sup>. Recently, it has also been shown that USC to a continuum could be simulated in superconducting circuits<sup>168</sup>, extending the method implemented in REF.<sup>103</sup> for simulation of USC to a cavity.

Ultrastrong coupling modifies the physics of an atom in a waveguide dramatically compared with when the coupling is low enough for the RWA to be applicable. Similar to the cavity case, the ground state contains a cloud of virtual photons (in many modes) surrounding the atom<sup>167,169</sup> and the atom transition frequency experiences a strong Lamb shift<sup>163,164,170,171</sup>. This considerably changes the transmission of photons in the waveguide; the standard scenario, in which the atom reflects single photons on resonance<sup>172</sup>, no longer holds<sup>167,170,171,173</sup> (FIG. 6a). Instead, similar to the nonlinear-optics-like processes<sup>20</sup> discussed below, the counter-rotating terms allow various frequency-conversion processes<sup>170,174,175</sup> (FIG. 6c). Other new phenomena include decreasing spontaneous emission rate with increasing coupling<sup>171</sup> and spontaneous emission of Schrödinger's cat states<sup>173</sup>.

### Connections to other models

The quantum Rabi Hamiltonian is closely related to a number of other fundamental models and emerging phenomena. These include the Hopfield model, a Jahn-Teller model<sup>58,165,176–178</sup>, a fluctuating-gap model of a disordered Peierls chain<sup>179</sup> and renormalization-group models, such as the spin-boson<sup>166,168</sup> and Kondo models<sup>166,169,175</sup>. The latter two models can be simulated by superconducting-circuit setups (FIG. 6a). It is counter-intuitive, but well-known, that purely electronic phenomena (such as the Kondo effect) are closely related to strongly dissipative two-level systems<sup>163,164</sup>.

Light-matter systems described by a generalized version of the quantum Rabi model (equation B1.1 in BOX 1 with  $g_1 \neq g_2$ ) enable quantum simulations of supersymmetrical field theories. Specifically, SUSY can be simulated with coupled resonators, each described by the quantum Rabi model and tuned to a SUSY point (or line)<sup>50</sup>. The quantum Rabi model naturally reveals a certain Bose–Fermi duality, which is the central concept of SUSY. This approach enables topologically protected

subspaces to be found, which may help to implement decoherence-free algorithms for QIP. Furthermore, a connection to SUSY breaking has been made for  $g_1 = g_2$  when the coupling grows large<sup>180</sup>. Moreover, dark matter in cosmology may be explained through SUSY, so superconducting quantum circuits in the USC regime could in principle realize dark-matter simulations on a chip.

The quantum Rabi model is also equivalent to a Rashba–Dresselhaus model, describing, for example, a 2D electron gas with spin-orbit coupling of Rashba and Dresselhaus types interacting with a perpendicular, constant magnetic field<sup>50</sup>. This is a fundamental model of condensed-matter physics, which can be realized in many other systems, such as semiconductor heterostructures, quantum wires, quantum dots (confined in parabolic potentials), carbon-based materials, 2D topological insulators, Weyl semimetals and ultracold neutral atoms.

Furthermore, a superconducting quantum circuit with USC has been suggested for demonstrating vacuum-induced symmetry breaking<sup>181</sup>. This effect is analogous to the Higgs mechanism for the generation of masses of weak-force gauge bosons through gauge-symmetry breaking.

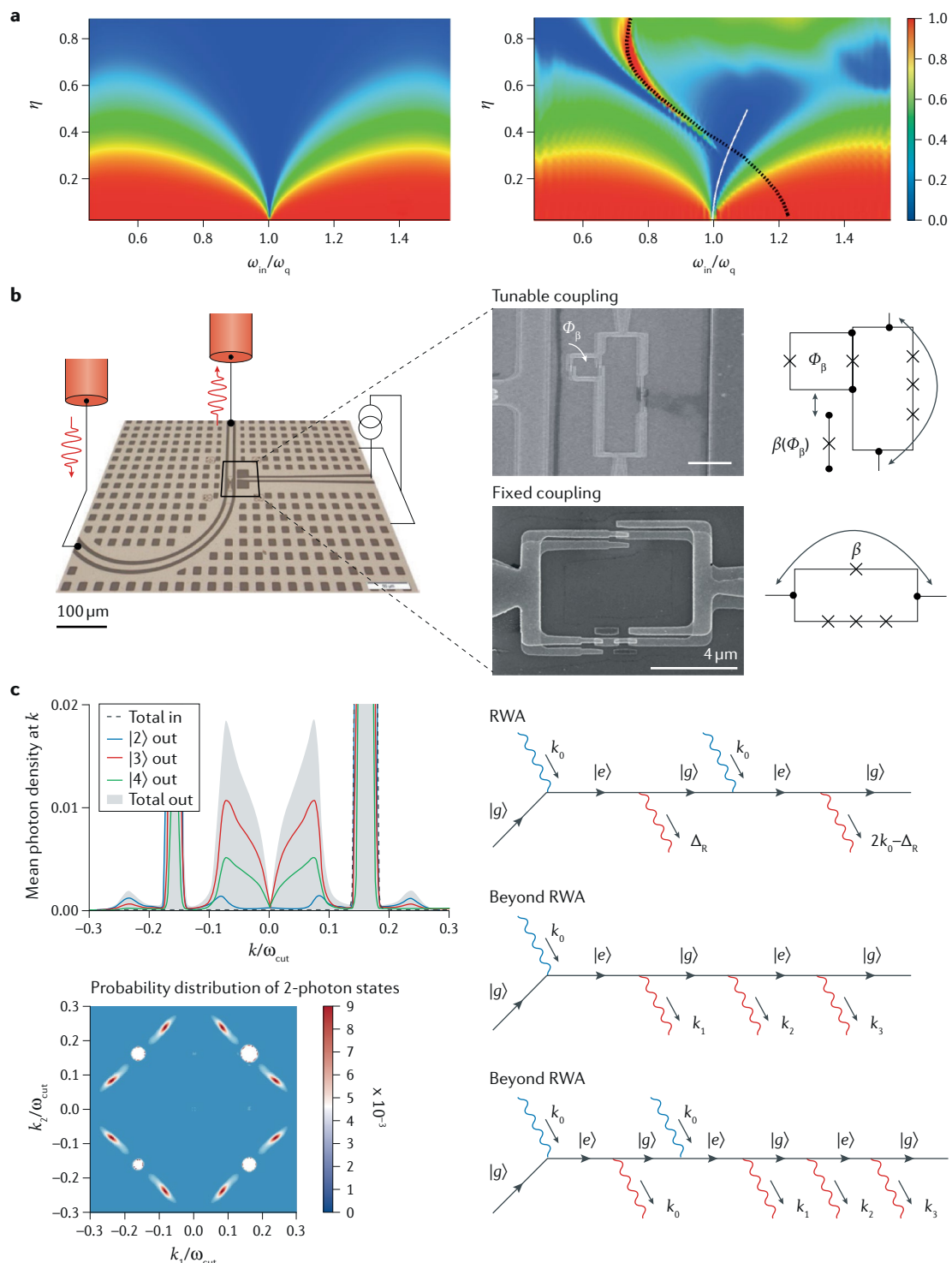
### Applications

Why do we need USC when we already have SC? The simplest answer is that USC enables more efficient interactions. For example, the coupling between a single photon and a single emitter results in significant nonlinearity, which has been used in electro-optical devices operating in the SC regime. Increasing  $\eta$  from SC to USC results in better performance of such devices, for example, faster control and response even for shorter lifetimes of the device components. Some quantum effects (including quantum gates) in specific realistic short-lifetime systems cannot be observed below USC.

The list of emerging applications of USC is much longer: QIP, quantum metrology, nonlinear optics, quantum optomechanics, quantum plasmonics, superconductivity, metamaterials, quantum field theory, quantum thermodynamics and even chemistry QED and materials science. Below, we discuss some of these applications in greater detail.

Another question is whether it is possible to predict and observe entirely new phenomena in the USC or DSC regimes. A simple example is the experimental observation of new stable states of matter. These states could be entangled hybrid light–matter ground states in the DSC regime<sup>41</sup> (FIG. 2), or discrete time crystals, which have been predicted<sup>182</sup> to exist in systems described by the Dicke model with tunable USC.

**Quantum information processing.** Cavity- and circuit-QED systems in the USC regime are especially useful for quantum technologies such as quantum metrology (an example is novel high-resolution spectroscopy<sup>183</sup> using smaller linewidths and improved signal-to-noise ratio) and QIP. For QIP, coherent transfer of excitations between light and matter is particularly important. Such transfer can be achieved in the SC regime, but it can be



much more efficient in the USC regime. Other QIP applications of USC include extremely fast quantum gate operations<sup>184,185</sup>, efficient realizations of quantum error correction<sup>186</sup>, quantum memories<sup>187,188</sup> (FIG. 7a), protected QIP<sup>189</sup> (FIG. 7b) and holonomic QIP<sup>190</sup>. The advantages are not only shorter operation times, but also simpler protocols, in which the natural evolution of a USC system replaces a sequence of quantum gates<sup>186</sup>. Some of these proposals also exploit the entangled ground states and parity symmetry.

**Modifying standard quantum phenomena.** Increasing  $\eta$  from SC to USC, various standard quantum phenomena often change drastically. Examples include the Purcell effect<sup>30</sup>, electromagnetically induced transparency and photon blockade<sup>66,120</sup>, spontaneous emission spectra<sup>191</sup>, the Zeno effect<sup>192,193</sup>, refrigeration in quantum thermodynamics<sup>194</sup> (FIG. 7c) and photon transfer in coupled cavities<sup>195</sup>. Such modified effects open up new emerging applications. In particular, light-induced topology<sup>196–198</sup> and quantum plasmonics<sup>199</sup> with SC can, in principle, be

**◀ Fig. 6 | Experiments and theory for ultrastrong coupling of an atom to an open waveguide.** **a** | Elastic transmission of a single photon at frequency  $\omega_{\text{in}}$ , travelling in an open waveguide coupled to a qubit with frequency  $\omega_q$ , as a function of normalized coupling strength  $\eta^{170}$ . The left panel shows the result using the rotating-wave approximation (RWA); the right panel shows the result including the counter-rotating terms in the Hamiltonian. On resonance the single photon is completely reflected by the qubit. The white curve shows the estimated position for the transmittance minimum, which is blueshifted. The dashed black curve marks the position of a Fano resonance that develops as the coupling increases and the effective qubit frequency is redshifted. **b** | The experimental setup that first achieved ultrastrong coupling (USC) to an open waveguide<sup>99</sup>. The coplanar waveguide, passing from the input line on the left of the chip to the output line at the top of the chip is interrupted by a loop containing Josephson junctions (crosses in the zoom-in). This loop forms the superconducting flux qubit. By adding a second loop (upper part of the right panel), the coupling strength can be tuned in situ by an external magnetic flux  $\Phi_\beta$  that modifies the coupling junction  $\beta$ . **c** | Frequency conversion in off-resonant scattering from a qubit with USC to an open waveguide<sup>174</sup>. The upper panel shows the scattered photon density at momentum  $k$  for a coherent input state at  $k_0 = 0.16 \omega_{\text{cut}}$  (dashed black curve, mean photon number  $\bar{n} = 0.5$ ) impinging on a qubit with renormalized frequency  $\omega_{q,\text{re}} = 0.08 \omega_{\text{cut}}$ , where  $\omega_{\text{cut}}$  is the cut-off frequency for the density of states in the waveguide. The blue, red, and green curves show that there are 2-, 3-, and 4-photon states, respectively, in the scattered signal. The lower panel shows the probability distribution of the two-photon states as a function of the photon momenta  $k_1$  and  $k_2$ . The right panel shows Feynman diagrams demonstrating how the counter-rotating terms in the Hamiltonian (neglected in the RWA) allow more frequency-conversion processes. Panel **a** is reproduced from REF.<sup>99</sup>, Springer Nature Limited. Panel **b** is reproduced with permission from REF.<sup>170</sup>, APS. Panel **c** is reproduced with permission from REF.<sup>174</sup>, APS.

improved and diversified with USC. Another intriguing development is that USC may help in understanding unconventional superconductivity through studies of light-enhanced (that is, polaritonically enhanced)<sup>200</sup> and photon-mediated<sup>201</sup> superconductivity.

**Higher-order processes and nonlinear optics.** The inclusion of the counter-rotating terms in the quantum Rabi Hamiltonian also enables prediction of higher-order processes. A prominent example is deterministic nonlinear optics (or vacuum-boosted nonlinear optics) with two-level atoms and (mostly) virtual photons in resonator modes<sup>20,186,202</sup>. These implementations, in contrast to conventional realizations of various multi-wave mixing processes in nonlinear optics, can reach perfect efficiency, need only a minimal number of photons and require only two atomic levels. The counter-rotating terms can also be leveraged in USC optomechanics to rapidly construct mechanical quantum states<sup>203</sup> (FIG. 7d) or observe the dynamical Casimir effect<sup>140</sup>.

Many nonlinear-optics processes can be described in terms of higher-order perturbation theory involving virtual transitions, in which the system passes from an initial state  $|i\rangle$  to the final state  $|f\rangle$  via a number of virtual transitions to intermediate states. These virtual transitions do not need to conserve energy, but their sum, the transition from  $|i\rangle$  to  $|f\rangle$ , does. When the light-matter coupling strength increases, the vacuum fluctuations of the electromagnetic field become able to induce such virtual transitions, replacing the role of the intense applied fields in nonlinear optics. In this way, higher-order processes involving counter-rotating terms can create an effective coupling between two states of the system ( $|i\rangle$  and  $|f\rangle$ ) with different numbers of excitations<sup>20</sup>. The strength of the effective coupling  $g_{\text{eff}}$  approximately scales as  $gn^n$ , where  $n$  is the number of intermediate virtual

states visited by the system on the way between  $|i\rangle$  and  $|f\rangle$  (an  $(n+1)$ th-order process).

If the light-matter coupling is sufficiently strong,  $g_{\text{eff}}$  becomes larger than the relevant decoherence rates in the system (that is, the effective coupling can be termed strong). In this case, the resulting coupling is deterministic, a highly desirable feature for practical applications in quantum technologies. Such a resonant coupling between two states with different numbers of excitations was observed in one of the first USC experiments in 2010 (REF.<sup>12</sup>).

Subsequent theoretical investigations have shown that these higher-order processes can give rise to intriguing novel cavity-QED effects, such as anomalous quantum Rabi oscillations, in which a two-level atomic transition can coherently emit or absorb photon pairs or triplets<sup>204,205</sup> (FIG. 7e), or multiple atoms jointly absorb or emit a single photon, each atom taking or providing part of the photon energy<sup>206</sup>. These deterministic processes enrich the possibilities of using cavity-QED for the development of efficient protocols for quantum technologies.

As discussed, superconducting quantum circuits with USC can also be used to simulate other fundamental models and test their predictions, for example, in quantum field theory and solid-state physics. We believe that these applications of the quantum Rabi model to other fundamental models in various branches of physics can stimulate research in all these fields by finding new analogues of condensed-matter effects in quantum-optical systems and vice versa.

**Chemistry with ultrastrong coupling.** There is increasing interest, theoretical and experimental, in the study of SC and USC cavity QED with molecular ensembles. This may lead to new routes to control chemical bonds and reactions (including dynamics, kinetics and thermodynamics) at the nanoscale level. Such photochemistry of molecular polaritons in optical cavities<sup>17,207,208</sup> is sometimes referred to as cavity<sup>209</sup> (or cavity-controlled<sup>18</sup>) chemistry, polariton chemistry<sup>200,210</sup> or QED chemistry<sup>211,212</sup>. This interest was partially triggered by an experiment that demonstrated the control of the coupling (from WC to USC) between photochromic spiropyran molecules and light in a low-Q metallic cavity<sup>11</sup>. In this and related experiments<sup>207</sup>, USC was reached by the collective coupling of many molecules to the cavity mode. To achieve USC (or even only SC) for a single molecule is much more demanding<sup>213</sup>.

Recent studies show that the excited-state reactivity of photochemical processes (such as catalysis and photosynthesis) in molecules in nanocavities can be substantially modified by SC and USC<sup>17,18,210,214</sup>. The reason is that  $g$  is comparable to the energies of vibrational and electronic transitions in molecules and their coupling<sup>17</sup>. In particular, a better control of chemical reactions can be realized via polaron decoupling, induced by SC or USC, of electronic and nuclear degrees of freedom in a molecular ensemble<sup>18</sup>. Possibilities and limitations of applying USC to change the electronic ground state of a molecular ensemble to control chemical reactions have also been investigated<sup>17,210</sup>. Some molecular observables depend solely on single-molecule couplings, whereas

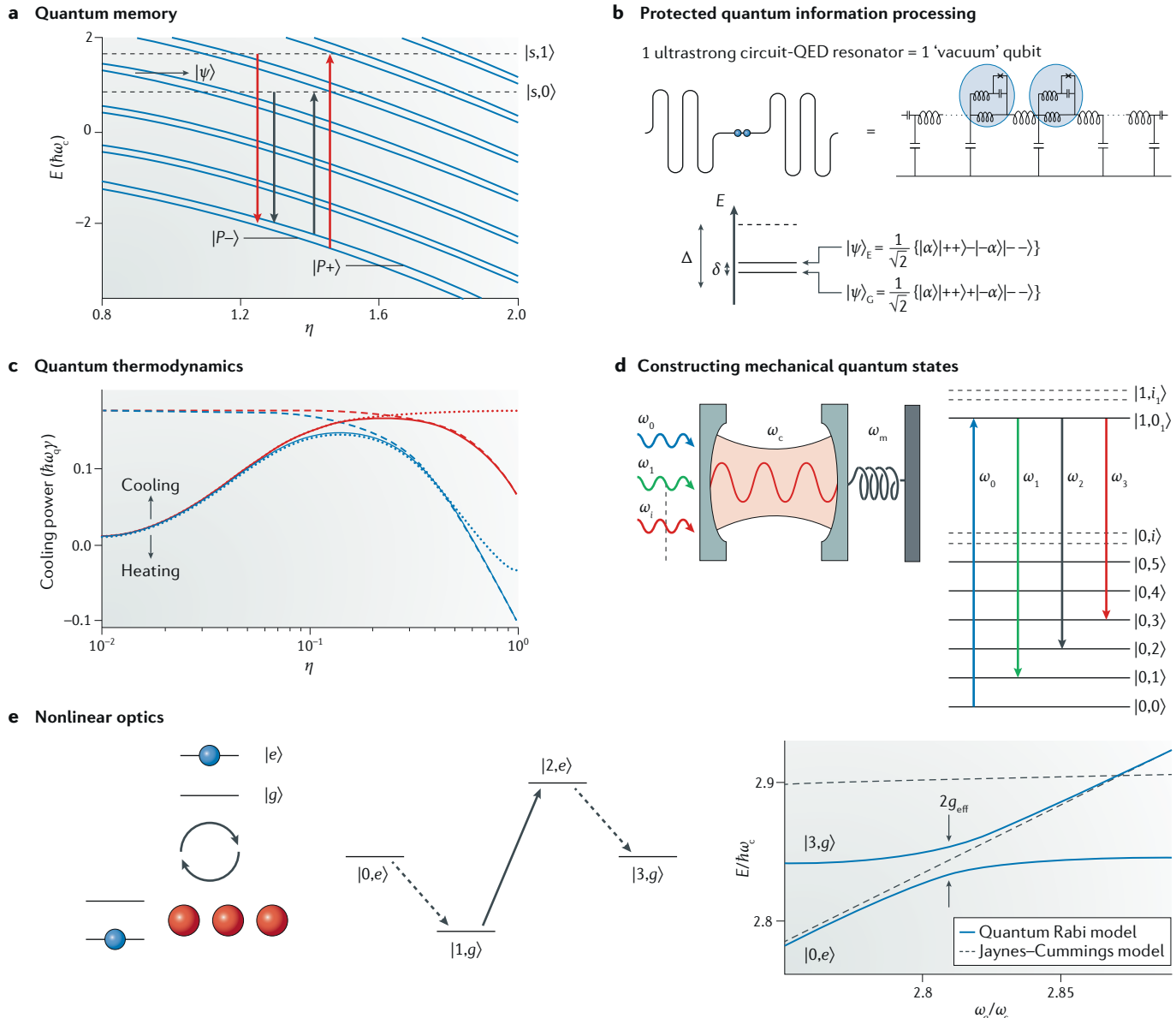


**Fig. 7 | Some potential applications of ultrastrong coupling.** **a** | Quantum memory. In a setup similar to that of panel **b**<sup>189</sup>, the two lowest energy levels  $|P_{\pm}\rangle$  of a qubit-resonator system in the deep-strong-coupling (DSC) regime make a good quantum memory<sup>187</sup>. Reading and writing a state  $|\psi\rangle$  in the memory is done via an auxiliary atomic level  $|s\rangle$  (see also FIG. 4c).  $\omega_c$  is the frequency of the cavity and  $\eta$  the normalized coupling strength. **b** | Protected quantum information processing (QIP). It was suggested<sup>189</sup> to use  $N$  qubits ( $N=2$  in the figure, which shows superconducting qubits and a transmission-line resonator) ultrastrongly coupled to a resonator to form computational states robust against decoherence. For high  $\eta$ , the ground and first excited states of the combined system are entangled coherent resonator states and  $\hat{\sigma}_x$  eigenstates of the qubits (see also FIG. 2e). These two states form a computational subspace that is well separated from other energy levels and protected, to a degree exponentially increasing with  $\eta$ , from certain decoherence mechanisms. **c** | Quantum thermodynamics. Cooling power as a function of  $\eta$  for a refrigeration system consisting of three coupled qubits (work, hot and cold)<sup>194</sup>. Red curves are results using the rotating-wave approximation (RWA) for the coupling, whereas blue curves are results with all coupling terms included; clearly the full coupling is needed to understand the cooling at high  $\eta$ . Solid curves are calculated using the correct master-equation treatment for ultrastrong coupling

(USC; BOX 3), whereas dashed and dotted curves show the result of standard approaches. **d** | In an optomechanical system (a cavity with frequency  $\omega_c$  and a moving mechanical mirror with frequency  $\omega_m \ll \omega_c$ ), an arbitrary mechanical state can be constructed in a single step when the strength of light-matter coupling  $g \approx \omega_c$  (REF<sup>203</sup>). A photonic excitation at frequency  $\omega_0$  can be converted into a superposition of mechanical Fock states by simultaneous drives at  $\omega_i$  that stimulate transitions. **e** | Nonlinear optics. The left panel shows a schematic depiction of a three-photon Rabi oscillation<sup>204</sup>, in which a single two-level atom emits and absorbs three photons. The middle panel shows the virtual transitions in the third-order process that converts the initial state  $|i\rangle = |0, e\rangle$  into the final state  $|f\rangle = |3, g\rangle$ . Dashed arrows are transitions mediated by terms in the Jaynes–Cummings Hamiltonian and solid arrows are transitions mediated by the counter-rotating terms in the quantum Rabi Hamiltonian. The right panel shows energy levels as a function of the atomic transition frequency  $\omega_q$ . The effective coupling between  $|i\rangle$  and  $|f\rangle$  on resonance is revealed by the avoided level crossing, which occurs for the quantum Rabi Hamiltonian, but is not present in the Jaynes–Cummings Hamiltonian. Panel **a** is reproduced with permission from REF.<sup>189</sup>, APS. Panel **b** is reproduced with permission from REF.<sup>194</sup>, APS. Panel **c** is reproduced with permission from REF.<sup>187</sup>, APS. Panel **d** is reproduced with permission from REF.<sup>203</sup>, APS.

others (such as those related to electronically excited states) can also be modified by collective couplings. Moreover, low-barrier chemical reactions can be affected by the quantum interference of different reaction pathways occurring simultaneously in multiple molecules ultrastrongly coupled to a cavity<sup>210</sup>.

Some of these studies<sup>208,209</sup> were based on the quantum Rabi model as in the standard quantum-optical approach. The Dicke model with anti-resonant terms was applied to the study of many molecules coupled to a surface plasmon<sup>210</sup>. Some other works<sup>212</sup> used a powerful QED density-functional formalism of QED chemistry<sup>211</sup>. This formalism unifies quantum optics and electronic-structure theories by treating a QED system composed of matter and light as a quantum liquid. The original formalism works well for SC, but becomes much less efficient in the USC regime<sup>212</sup>.

## Conclusion and outlook

As we describe in this Review, many intriguing physical effects have been predicted in the USC regime of light-matter interaction. However, related experiments have been limited to increasing the light-matter coupling strength and verifying it by standard transmission measurements. Now that USC has been reached in a broad range of systems, we believe that it is time to experimentally explore the new interesting phenomena specific to USC and, finally, to find their useful applications. A few decades ago, cavity QED in the WC and SC regimes was following the same route, which led to important applications in modern quantum technologies. We believe that USC applications also have the potential to make a profound impact.

Published online 8 January 2019

1. Purcell, E. M. Spontaneous emission probabilities at radio frequencies. *Phys. Rev.* **69**, 681 (1946).
2. Kaluzny, Y., Goy, P., Gross, M., Raimond, J. M. & Haroche, S. Observation of self-induced Rabi oscillations in two-level atoms excited inside a resonant cavity: the ringing regime of superradiance. *Phys. Rev. Lett.* **51**, 1175 (1983).
3. Meschede, D., Walther, H. & Müller, G. One-atom maser. *Phys. Rev. Lett.* **54**, 551 (1985).
4. Thompson, R. J., Rempe, G. & Kimble, H. J. Observation of normal-mode splitting for an atom in an optical cavity. *Phys. Rev. Lett.* **68**, 1132 (1992).
5. Weisbuch, C., Nishioka, M., Ishikawa, A. & Arakawa, Y. Observation of the coupled exciton-photon mode splitting in a semiconductor quantum microcavity. *Phys. Rev. Lett.* **69**, 3314 (1992).
6. Lodahl, P., Mahmoodian, S. & Stobbe, S. Interfacing single photons and single quantum dots with photonic nanostructures. *Rev. Mod. Phys.* **87**, 347 (2015).
7. Gu, X., Kockum, A. F., Miranowicz, A., Liu, Y.-X. & Nori, F. Microwave photonics with superconducting quantum circuits. *Phys. Rep.* **718–719**, 1–102 (2017).
8. Dicke, R. H. Coherence in spontaneous radiation processes. *Phys. Rev.* **93**, 99 (1954).
9. Devoret, M. H., Girvin, S. & Schoelkopf, R. Circuit-QED: how strong can the coupling between a Josephson junction atom and a transmission line resonator be? *Ann. Phys.* **16**, 767 (2007).
10. Ciuti, C., Bastard, G. & Carusotto, I. Quantum vacuum properties of the intersubband cavity polariton field. *Phys. Rev. B* **72**, 115303 (2005).
11. Anappara, A. A. et al. Signatures of the ultrastrong light-matter coupling regime. *Phys. Rev. B* **79**, 201303 (2009).
12. Niemczyk, T. et al. Circuit quantum electrodynamics in the ultrastrong-coupling regime. *Nat. Phys.* **6**, 772 (2010).
13. Forn-Díaz, P. et al. Observation of the Bloch-Siegert shift in a qubit-oscillator system in the ultrastrong coupling regime. *Phys. Rev. Lett.* **105**, 237001 (2010).
14. Gambino, S. et al. Exploring light-matter interaction phenomena under ultrastrong coupling regime. *ACS Photonics* **1**, 1042 (2014).
15. Genco, A. et al. Bright polariton coumarin-based OLEDs operating in the ultrastrong coupling regime. *Adv. Opt. Mater.* **6**, 1800364 (2018).
16. Ashhab, S. & Nori, F. Qubit-oscillator systems in the ultrastrong-coupling regime and their potential for preparing nonclassical states. *Phys. Rev. A* **81**, 042311 (2010).
17. Galego, J., García-Vidal, F. J. & Feist, J. Cavity-induced modifications of molecular structure in the strong-coupling regime. *Phys. Rev. X* **5**, 041022 (2015).
18. Herrera, F. & Spano, F. C. Cavity-controlled chemistry in molecular ensembles. *Phys. Rev. Lett.* **116**, 238301 (2016).
19. Cirio, M., De Liberato, S., Lambert, N. & Nori, F. Ground state electroluminescence. *Phys. Rev. Lett.* **116**, 113601 (2016).
20. Kockum, A. F., Miranowicz, A., Macri, V., Savasta, S. & Nori, F. Deterministic quantum nonlinear optics with single atoms and virtual photons. *Phys. Rev. A* **95**, 063849 (2017).
21. Bayer, A. et al. Terahertz light-matter interaction beyond unity coupling strength. *Nano. Lett.* **17**, 6340 (2017).
22. Vahala, K. J. Optical microcavities. *Nature* **424**, 839 (2003).
23. Shields, A. J. Semiconductor quantum light sources. *Nat. Photonics* **1**, 215 (2007).
24. Salter, C. L. et al. An entangled-light-emitting diode. *Nature* **465**, 594 (2010).
25. Haroche, S. Nobel lecture: controlling photons in a box and exploring the quantum to classical boundary. *Rev. Mod. Phys.* **85**, 1083 (2013).
26. Georgescu, I. & Nori, F. Quantum technologies: an old new story. *Phys. World* **25**, 16 (2012).
27. Degen, C. L., Reinhard, F. & Cappellaro, P. Quantum sensing. *Rev. Mod. Phys.* **89**, 035002 (2017).
28. Wendin, G. Quantum information processing with superconducting circuits: a review. *Rep. Prog. Phys.* **80**, 106001 (2017).
29. De Liberato, S. Virtual photons in the ground state of a dissipative system. *Nat. Commun.* **8**, 1465 (2017).
30. De Liberato, S. Light-matter decoupling in the deep strong coupling regime: the breakdown of the Purcell effect. *Phys. Rev. Lett.* **112**, 016401 (2014).
31. Sundaresan, N. M. et al. Beyond strong coupling in a multimode cavity. *Phys. Rev. X* **5**, 021035 (2015).
32. George, J. et al. Multiple Rabi splittings under ultrastrong vibrational coupling. *Phys. Rev. Lett.* **117**, 153601 (2016).
33. Bosman, S. J. et al. Multi-mode ultra-strong coupling in circuit quantum electrodynamics. *npj Quantum Inf.* **3**, 46 (2017).
34. Gely, M. F. et al. Convergence of the multimode quantum Rabi model of circuit quantum electrodynamics. *Phys. Rev. B* **95**, 245115 (2017).
35. Sánchez Muñoz, C., Nori, F. & De Liberato, S. Resolution of superluminal signalling in non-perturbative cavity quantum electrodynamics. *Nat. Commun.* **9**, 1924 (2018).
36. De Bernardis, D., Jaako, T. & Rabl, P. Cavity quantum electrodynamics in the nonperturbative regime. *Phys. Rev. A* **97**, 043820 (2018).
37. De Bernardis, D., Pilar, P., Jaako, T., De Liberato, S. & Rabl, P. Breakdown of gauge invariance in ultrastrong-coupling cavity QED. *Phys. Rev. A* **98**, 053819 (2018).
38. Di Stefano, O. et al. Resolution of gauge ambiguities in ultrastrong-coupling cavity QED. Preprint at <http://arxiv.org/abs/1809.08749> (2018).
39. Jaynes, E. T. & Cummings, F. W. Comparison of quantum and semiclassical radiation theories with application to the beam maser. *Proc. IEEE* **51**, 89 (1963).
40. Shore, B. W. & Knight, P. L. The Jaynes-Cummings model. *J. Mod. Opt.* **40**, 1195 (1993).
41. Yoshihara, F. et al. Superconducting qubit-oscillator circuit beyond the ultrastrong-coupling regime. *Nat. Phys.* **13**, 44 (2017).
42. Braak, D. Integrability of the Rabi model. *Phys. Rev. Lett.* **107**, 100401 (2011).
43. Braak, D. Solution of the Dicke model for  $N = 3$ . *J. Phys. B. At. Mol. Opt. Phys.* **46**, 224007 (2013).
44. Peng, J., Ren, Z., Guo, G., Ju, G. & Guo, X. Exact solutions of the generalized two-photon and two-qubit Rabi models. *Eur. Phys. J. D* **67**, 162 (2013).
45. Chilengaryan, S. A. & Rodríguez-Lara, B. M. Exceptional solutions in two-mode quantum Rabi models. *J. Phys. B. At. Mol. Opt. Phys.* **48**, 245501 (2015).
46. Qin, W. et al. Exponentially enhanced light-matter interaction, cooperativities, and steady-state entanglement using parametric amplification. *Phys. Rev. Lett.* **120**, 093601 (2018).
47. Leroux, C., Govia, L. C. G. & Clerk, A. A. Enhancing cavity quantum electrodynamics via antisqueezing: synthetic ultrastrong coupling. *Phys. Rev. Lett.* **120**, 093602 (2018).
48. Tavis, M. & Cummings, F. W. Exact solution for an  $N$ -molecule-radiation-field Hamiltonian. *Phys. Rev.* **170**, 379 (1968).
49. Bloch, F. & Siegert, A. Magnetic resonance for non-rotating fields. *Phys. Rev.* **57**, 224 (1940).
50. Tomka, M., Pletyukhov, M. & Gritsev, V. Supersymmetry in quantum optics and in spin-orbit coupled systems. *Sci. Rep.* **5**, 13097 (2015).
51. Hagenmüller, D., De Liberato, S. & Ciuti, C. Ultrastrong coupling between a cavity resonator and the cyclotron transition of a two-dimensional electron gas in the case of an integer filling factor. *Phys. Rev. B* **81**, 235303 (2010).
52. Zhang, Q. et al. Collective non-perturbative coupling of 2D electrons with high-quality-factor terahertz cavity photons. *Nat. Phys.* **12**, 1005 (2016).
53. Li, X. et al. Vacuum Bloch-Siegert shift in Landau polaritons with ultra-high cooperativity. *Nat. Photonics* **12**, 324 (2018).
54. Casanova, J., Romero, G., Lizuain, I., García-Ripoll, J. J. & Solano, E. Deep strong coupling regime of the Jaynes-Cummings model. *Phys. Rev. Lett.* **105**, 263603 (2010).

55. Khurgin, J. B. Excitonic radius in the cavity polariton in the regime of very strong coupling. *Solid State Commun.* **117**, 307 (2001).
56. Brodbeck, S. et al. Experimental verification of the very strong coupling regime in a GaAs quantum well microcavity. *Phys. Rev. Lett.* **119**, 027401 (2017).
57. Moores, B. A., Sletten, L. R., Viennot, J. J. & Lehnert, K. W. Cavity quantum acoustic device in the multimode strong coupling regime. *Phys. Rev. Lett.* **120**, 227701 (2018).
58. Hines, A. P., Dawson, C. M., McKenzie, R. H. & Milburn, G. J. Entanglement and bifurcations in Jahn-Teller models. *Phys. Rev. A* **70**, 022303 (2004).
59. Hepp, K. & Lieb, E. H. On the superradiant phase transition for molecules in a quantized radiation field: the Dicke maser model. *Ann. Phys. (N. Y.)* **76**, 360 (1973).
60. Wang, Y. K. & Hioe, F. T. Phase transition in the Dicke model of superradiance. *Phys. Rev. A* **7**, 831 (1973).
61. Emary, C. & Brandes, T. Chaos and the quantum phase transition in the Dicke model. *Phys. Rev. E* **67**, 066203 (2003).
62. Ashhab, S. & Sembra, K. Superradiance phase transition in the presence of parameter fluctuations. *Phys. Rev. A* **95**, 053833 (2017).
63. Ashhab, S. Superradiance transition in a system with a single qubit and a single oscillator. *Phys. Rev. A* **87**, 013826 (2013).
64. Quattropani, A., Andreani, L. C. & Bassani, F. Quantum theory of polaritons with spatial dispersion: exact solutions. *Nuovo Cim. D* **7**, 55 (1986).
65. Jaako, T., Xiang, Z.-L., García-Ripoll, J. J. & Rabl, P. Ultrastrong-coupling phenomena beyond the Dicke model. *Phys. Rev. A* **94**, 033850 (2016).
66. Le Boité, A., Hwang, M.-J., Nha, H. & Plenio, M. B. Fate of photon blockade in the deep strong-coupling regime. *Phys. Rev. A* **94**, 033827 (2016).
67. Hagenmüller, D. & Ciuti, C. Cavity QED of the graphene cyclotron transition. *Phys. Rev. Lett.* **109**, 267403 (2012).
68. Nataf, P. & Ciuti, C. No-go theorem for superradiant quantum phase transitions in cavity QED and counter-example in circuit QED. *Nat. Commun.* **1**, 72 (2010).
69. Viehmann, O., von Delft, J. & Marquardt, F. Superradiant phase transitions and the standard description of circuit QED. *Phys. Rev. Lett.* **107**, 113602 (2011).
70. Chiroli, L., Polini, M., Giovannetti, V. & MacDonald, A. H. Drude weight, cyclotron resonance, and the Dicke model of graphene cavity QED. *Phys. Rev. Lett.* **109**, 267404 (2012).
71. Tufarelli, T., McEnergy, K. R., Maier, S. A. & Kim, M. S. Signatures of the A<sup>2</sup> term in ultrastrongly coupled oscillators. *Phys. Rev. A* **91**, 063840 (2015).
72. García-Ripoll, J. J., Peropadre, B. & De Liberato, S. Light-matter decoupling and A<sup>2</sup> term detection in superconducting circuits. *Sci. Rep.* **5**, 16055 (2015).
73. Rossi, M. A. C. et al. Probing the diamagnetic term in light-matter interaction. *Quantum Sci. Technol.* **2**, 01LT01 (2017).
74. Rzażewski, K., Wódkiewicz, K. & źakowicz, W. Phase transitions, two-level atoms, and the A<sup>2</sup> term. *Phys. Rev. Lett.* **35**, 432 (1975).
75. Slyusarev, V. A. & Yankelevich, R. P. On the impossibility of a phase transition to the superradiant state in a thermodynamically equilibrium gauge-invariant system. *Theor. Math. Phys.* **40**, 641 (1979).
76. Keeling, J. Coulomb interactions, gauge invariance, and phase transitions of the Dicke model. *J. Phys. Condens. Matter* **19**, 295213 (2007).
77. Vukics, A. & Domokos, P. Adequacy of the Dicke model in cavity QED: a counter-no-go statement. *Phys. Rev. A* **86**, 053807 (2012).
78. Baksic, A., Nataf, P. & Ciuti, C. Superradiant phase transitions with three-level systems. *Phys. Rev. A* **87**, 023813 (2013).
79. Vukics, A., Grießer, T. & Domokos, P. Elimination of the A-square problem from cavity QED. *Phys. Rev. Lett.* **112**, 073601 (2014).
80. Bamba, M. & Ogawa, T. Stability of polarizable materials against superradiant phase transition. *Phys. Rev. A* **90**, 063825 (2014).
81. Bamba, M. & Imoto, N. Circuit configurations which may or may not show superradiant phase transitions. *Phys. Rev. A* **96**, 053857 (2017).
82. Todorov, Y. & Sirtori, C. Intersubband polaritons in the electrical dipole gauge. *Phys. Rev. B* **85**, 045304 (2012).
83. De Liberato, S. & Ciuti, C. Quantum theory of intersubband polarons. *Phys. Rev. B* **85**, 125302 (2012).
84. De Liberato, S. & Ciuti, C. Quantum phases of a multimode bosonic field coupled to flat electronic bands. *Phys. Rev. Lett.* **110**, 133603 (2013).
85. Askenazi, B. et al. Ultra-strong light-matter coupling for designer Reststrahlen band. *New J. Phys.* **16**, 043029 (2014).
86. Askenazi, B. et al. Midinfrared ultrastrong light-matter coupling for THz thermal emission. *ACS Photonics* **4**, 2550 (2017).
87. Günter, G. et al. Sub-cycle switch-on of ultrastrong light-matter interaction. *Nature* **458**, 178 (2009).
88. De Liberato, S., Ciuti, C. & Carusotto, I. Quantum vacuum radiation spectra from a semiconductor microcavity with a time-modulated vacuum Rabi frequency. *Phys. Rev. Lett.* **98**, 103602 (2007).
89. Auer, A. & Burkard, G. Entangled photons from the polariton vacuum in a switchable optical cavity. *Phys. Rev. B* **85**, 235140 (2012).
90. Todorov, Y. et al. Ultrastrong light-matter coupling regime with polariton dots. *Phys. Rev. Lett.* **105**, 196402 (2010).
91. Jouy, P. et al. Transition from strong to ultrastrong coupling regime in mid-infrared metal-dielectric-metal cavities. *Appl. Phys. Lett.* **98**, 231114 (2011).
92. Geiser, M. et al. Ultrastrong coupling regime and plasmon polaritons in parabolic semiconductor quantum wells. *Phys. Rev. Lett.* **108**, 106402 (2012).
93. Delteil, A. et al. Charge-induced coherence between intersubband plasmons in a quantum structure. *Phys. Rev. Lett.* **109**, 246808 (2012).
94. Forn-Díaz, P., Romero, G., Harmans, C. J. P. M., Solano, E. & Mooij, J. E. Broken selection rule in the quantum Rabi model. *Sci. Rep.* **6**, 26720 (2016).
95. Baust, A. et al. Ultrastrong coupling in two-resonator circuit QED. *Phys. Rev. B* **93**, 214501 (2016).
96. Chen, Z. et al. Single-photon-driven high-order sideband transitions in an ultrastrongly coupled circuit-quantum-electrodynamics system. *Phys. Rev. A* **96**, 012325 (2017).
97. Yoshihara, F. et al. Characteristic spectra of circuit quantum electrodynamics systems from the ultrastrong-to-the deep-strong-coupling regime. *Phys. Rev. A* **95**, 053824 (2017).
98. Yoshihara, F. et al. Inversion of qubit energy levels in qubit-oscillator circuits in the deep-strong-coupling regime. *Phys. Rev. Lett.* **120**, 183601 (2018).
99. Forn-Díaz, P. et al. Ultrastrong coupling of a single artificial atom to an electromagnetic continuum in the nonperturbative regime. *Nat. Phys.* **13**, 39 (2017). **The first experiment to demonstrate ultrastrong coupling between a qubit and a continuum of light modes in an open waveguide.**
100. Magazzù, L. et al. Probing the strongly driven spin-boson model in a superconducting quantum circuit. *Nat. Commun.* **9**, 1403 (2018).
101. Puertas Martínez, J. et al. A tunable Josephson platform to explore many-body quantum optics in circuit-QED. Preprint at <http://arxiv.org/abs/1802.00633> (2018).
102. Langford, N. K. et al. Experimentally simulating the dynamics of quantum light and matter at deep-strong coupling. *Nat. Commun.* **8**, 1715 (2017). **Experimental quantum simulation of the quantum Rabi model, demonstrating photonic Schrödinger's cat states in the ground state of that model.**
103. Braumüller, J. et al. Analog quantum simulation of the Rabi model in the ultrastrong coupling regime. *Nat. Commun.* **8**, 779 (2017).
104. Scalari, G. et al. Ultrastrong coupling of the cyclotron transition of a 2D electron gas to a THz metamaterial. *Science* **335**, 1323 (2012).
105. Scalari, G. et al. Ultrastrong light-matter coupling at terahertz frequencies with split ring resonators and inter-Landau level transitions. *J. Appl. Phys.* **113**, 136510 (2013).
106. Maissen, C. et al. Ultrastrong coupling in the near field of complementary split-ring resonators. *Phys. Rev. B* **90**, 205309 (2014).
107. Keller, J. et al. Critical softening of cavity cyclotron polariton modes in strained germanium 2D hole gas in the ultra-strong coupling regime. Preprint at <http://arxiv.org/abs/1708.07773> (2017).
108. Muravev, V. M., Andreev, I. V., Kukushkin, I. V., Schmult, S. & Dietsche, W. Observation of hybrid plasmon-photon modes in microwave transmission of coplanar microresonators. *Phys. Rev. B* **83**, 075309 (2011).
109. Paravicini-Bagliani, G. L. et al. Tomography of an ultrastrongly coupled polariton state using magneto-transport in the quantum regime. *Nat. Phys.* <https://doi.org/10.1038/s41567-018-0346-y> (2018).
110. Todisco, F. et al. Ultrastrong plasmon-exciton coupling by dynamic molecular aggregation. *ACS Photonics* **5**, 143 (2018).
111. Schwartz, T., Hutchison, J. A., Genet, C. & Ebbesen, T. W. Reversible switching of ultrastrong light-molecule coupling. *Phys. Rev. Lett.* **106**, 196405 (2011).
112. Kéna-Cohen, S., Maier, S. A. & Bradley, D. D. C. Ultrastrongly coupled exciton-polaritons in metal-clad organic semiconductor microcavities. *Adv. Opt. Mater.* **1**, 827 (2013).
113. Gubbins, C. R., Maier, S. A. & Kéna-Cohen, S. Low-voltage polariton electroluminescence from an ultrastrongly coupled organic light-emitting diode. *Appl. Phys. Lett.* **104**, 233302 (2014).
114. Mazzeo, M. et al. Ultrastrong light-matter coupling in electrically doped microcavity organic light emitting diodes. *Appl. Phys. Lett.* **104**, 233303 (2014).
115. Barachati, F. et al. Tunable third-harmonic generation from polaritons in the ultrastrong coupling regime. *ACS Photonics* **5**, 119 (2018).
116. Eizirik, E., Brodeur, J., Barachati, F., Sridharan, A. & Kéna-Cohen, S. Organic photodiodes with an extended responsivity using ultrastrong light-matter coupling. *ACS Photonics* **5**, 2921 (2018).
117. Benz, F. et al. Single-molecule optomechanics in ‘picocavities’. *Science* **354**, 726 (2016).
118. Pirkkalainen, J.-M. et al. Cavity optomechanics mediated by a quantum two-level system. *Nat. Commun.* **6**, 6981 (2015).
119. Beaudoin, F., Gambetta, J. M. & Blais, A. Dissipation and ultrastrong coupling in circuit QED. *Phys. Rev. A* **84**, 043832 (2011).
120. Ridolfo, A., Leib, M., Savasta, S. & Hartmann, M. J. Photon blockade in the ultrastrong coupling regime. *Phys. Rev. Lett.* **109**, 193602 (2012).
121. Stassi, R., Savasta, S., Garziano, L., Spagnolo, B. & Nori, F. Output field-quadrature measurements and squeezing in ultrastrong cavity-QED. *New J. Phys.* **18**, 123005 (2016).
122. Ridolfo, A., Savasta, S. & Hartmann, M. J. Nonclassical radiation from thermal cavities in the ultrastrong coupling regime. *Phys. Rev. Lett.* **110**, 163601 (2013).
123. Garziano, L., Ridolfo, A., De Liberato, S. & Savasta, S. Cavity QED in the ultrastrong coupling regime: photon bunching from the emission of individual dressed qubits. *ACS Photonics* **4**, 2345 (2017).
124. Ciuti, C. & Carusotto, I. Input-output theory of cavities in the ultrastrong coupling regime: the case of time-independent cavity parameters. *Phys. Rev. A* **74**, 033811 (2006).
125. Savasta, S. & Girlanda, R. Quantum description of the input and output electromagnetic fields in a polarizable confined system. *Phys. Rev. A* **53**, 2716 (1996).
126. Di Stefano, O., Kokum, A. F., Ridolfo, A., Savasta, S. & Nori, F. Photodetection probability in quantum systems with arbitrarily strong light-matter interaction. *Sci. Rep.* **8**, 17825 (2018).
127. Lolli, J., Baksic, A., Nagy, D., Manucharyan, V. E. & Ciuti, C. Ancillary qubit spectroscopy of vacua in cavity and circuit quantum electrodynamics. *Phys. Rev. Lett.* **114**, 183601 (2015).
128. Cirio, M., Debnath, K., Lambert, N. & Nori, F. Amplified optomechanical transduction of virtual radiation pressure. *Phys. Rev. Lett.* **119**, 053601 (2017).
129. De Liberato, S., Gerace, D., Carusotto, I. & Ciuti, C. Extracavity quantum vacuum radiation from a single qubit. *Phys. Rev. A* **80**, 053810 (2009).
130. Takashima, K., Hatakenaka, N., Kurihara, S. & Zeilinger, A. Nonstationary boundary effect for a quantum flux in superconducting nanocircuits. *J. Phys. A Math. Theor.* **41**, 164036 (2008).
131. Werlang, T., Dodonov, A. V., Duzzioni, E. I. & Villas-Boas, C. J. Rabi model beyond the rotating-wave approximation: generation of photons from vacuum through decoherence. *Phys. Rev. A* **78**, 053805 (2008).
132. Dodonov, A. V., Celeri, L. C., Pascoal, F., Lukin, M. D. & Yelin, S. F. Photon generation from vacuum in non-stationary circuit QED. Preprint at <http://arxiv.org/abs/0806.4035> (2008).
133. Carusotto, I., De Liberato, S., Gerace, D. & Ciuti, C. Back-reaction effects of quantum vacuum in cavity quantum electrodynamics. *Phys. Rev. A* **85**, 023805 (2012).
134. Garziano, L., Ridolfo, A., Stassi, R., Di Stefano, O. & Savasta, S. Switching on and off of ultrastrong light-matter interaction: photon statistics of quantum vacuum radiation. *Phys. Rev. A* **88**, 063829 (2013).
135. Shapiro, D. S., Zhukov, A. A., Pogosov, W. V. & Lozovik, Y. E. Dynamical Lamb effect in a tunable

- superconducting qubit-cavity system. *Phys. Rev. A* **91**, 063814 (2015).
136. Moore, G. T. Quantum theory of the electromagnetic field in a variable-length one-dimensional cavity. *J. Math. Phys.* **11**, 2679 (1970).
  137. Johansson, J. R., Johansson, G., Wilson, C. M. & Nori, F. Dynamical Casimir effect in a superconducting coplanar waveguide. *Phys. Rev. Lett.* **103**, 147003 (2009).
  138. Wilson, C. M. et al. Observation of the dynamical Casimir effect in a superconducting circuit. *Nature* **479**, 376 (2011).
  139. Nation, P. D., Johansson, J. R., Blencowe, M. P. & Nori, F. Colloquium: Stimulating uncertainty: amplifying the quantum vacuum with superconducting circuits. *Rev. Mod. Phys.* **84**, 1 (2012).
  140. Macri, V. et al. Nonperturbative dynamical Casimir effect in optomechanical systems: vacuum Casimir-Rabi splittings. *Phys. Rev. X* **8**, 011031 (2018).
  141. Ridolfo, A., Vilardi, R., Di Stefano, O., Portolan, S. & Savasta, S. All optical switch of vacuum Rabi oscillations: the ultrafast quantum eraser. *Phys. Rev. Lett.* **106**, 013601 (2011).
  142. Huang, J.-F. & Law, C. K. Photon emission via vacuum-dressed intermediate states under ultrastrong coupling. *Phys. Rev. A* **89**, 033827 (2014).
  143. Di Stefano, O. et al. Feynman-diagrams approach to the quantum Rabi model for ultrastrong cavity QED: stimulated emission and reabsorption of virtual particles dressing a physical excitation. *New J. Phys.* **19**, 053010 (2017).
  144. Buluta, I. & Nori, F. Quantum simulators. *Science* **326**, 108 (2009).
  145. Georgescu, I. M., Ashhab, S. & Nori, F. Quantum simulation. *Rev. Mod. Phys.* **86**, 153 (2014).
  146. Baumann, K., Guerlin, C., Brennecke, F. & Esslinger, T. Dicke quantum phase transition with a superfluid gas in an optical cavity. *Nature* **464**, 1301 (2010).
  147. Longhi, S. Jaynes-Cummings photonic superlattices. *Opt. Lett.* **36**, 3407 (2011).
  148. Crespi, A., Longhi, S. & Osselame, R. Photonic realization of the quantum Rabi model. *Phys. Rev. Lett.* **108**, 163601 (2012).
  149. Dimer, F., Estienne, B., Parkins, A. S. & Carmichael, H. J. Proposed realization of the Dicke-model quantum phase transition in an optical cavity QED system. *Phys. Rev. A* **75**, 013804 (2007).
  150. Ballester, D., Romero, G., García-Ripoll, J. J., Deppe, F. & Solano, E. Quantum simulation of the ultrastrong-coupling dynamics in circuit quantum electrodynamics. *Phys. Rev. X* **2**, 021007 (2012).
  151. Grimsom, A. L. & Parkins, S. Cavity-QED simulation of qubit-oscillator dynamics in the ultrastrong-coupling regime. *Phys. Rev. A* **87**, 033814 (2013).
  152. Pedernales, J. S. et al. Quantum Rabi model with trapped ions. *Sci. Rep.* **5**, 15472 (2015).
  153. Felicetti, S. et al. Spectral collapse via two-phonon interactions in trapped ions. *Phys. Rev. A* **92**, 033817 (2015).
  154. Puebla, R., Hwang, M.-J., Casanova, J. & Plenio, M. B. Probing the dynamics of a superradiant quantum phase transition with a single trapped ion. *Phys. Rev. Lett.* **118**, 073001 (2017).
  155. Fedortchenko, S. et al. Quantum simulation of ultrastrongly coupled bosonic modes using superconducting circuits. *Phys. Rev. A* **95**, 042313 (2017).
  156. Aedo, I. & Lamata, L. Analog quantum simulation of generalized Dicke models in trapped ions. *Phys. Rev. A* **97**, 042317 (2018).
  157. Felicetti, S., Romero, G., Solano, E. & Sabín, C. Quantum Rabi model in a superfluid Bose-Einstein condensate. *Phys. Rev. A* **96**, 033839 (2017).
  158. Felicetti, S. et al. Quantum Rabi model in the Brillouin zone with ultracold atoms. *Phys. Rev. A* **95**, 013827 (2017).
  159. Lv, D. et al. Quantum Simulation of the quantum Rabi model in a trapped ion. *Phys. Rev. X* **8**, 021027 (2018).
  160. Markovic, D. et al. Demonstration of an effective ultrastrong coupling between two oscillators. *Phys. Rev. Lett.* **121**, 040505 (2018).
  161. Mezzacapo, A. et al. Digital quantum Rabi and Dicke models in superconducting circuits. *Sci. Rep.* **4**, 7482 (2014).
  162. Lamata, L. Digital-analog quantum simulation of generalized Dicke models with superconducting circuits. *Sci. Rep.* **7**, 43768 (2017).
  163. Leggett, A. J. et al. Dynamics of the dissipative two-state system. *Rev. Mod. Phys.* **59**, 1 (1987).
  164. Weiss, U. *Quantum Dissipative Systems*, 4th edn. (World Scientific, 2012).
  165. Bourassa, J. et al. Ultrastrong coupling regime of cavity QED with phase-biased flux qubits. *Phys. Rev. A* **80**, 032109 (2009).
  166. Le Hur, K. Kondo resonance of a microwave photon. *Phys. Rev. B* **85**, 140506 (2012).
  167. Peropadre, B., Zueco, D., Porras, D. & García-Ripoll, J. J. Nonequilibrium and nonperturbative dynamics of ultrastrong coupling in open lines. *Phys. Rev. Lett.* **111**, 243602 (2013).
  168. Leppäkangas, J. et al. Quantum simulation of the spin-boson model with a microwave circuit. *Phys. Rev. A* **97**, 052321 (2018).
  169. Snyman, I. & Florens, S. Robust Josephson-Kondo screening cloud in circuit quantum electrodynamics. *Phys. Rev. B* **92**, 085131 (2015).
  170. Sanchez-Burillo, E., Zueco, D., García-Ripoll, J. J. & Martin-Moreno, L. Scattering in the ultrastrong regime: nonlinear optics with one photon. *Phys. Rev. Lett.* **113**, 236304 (2014).
  171. Díaz-Camacho, G., Bermudez, A. & García-Ripoll, J. J. Dynamical polaron Ansatz: a theoretical tool for the ultrastrong-coupling regime of circuit QED. *Phys. Rev. A* **93**, 043843 (2016).
  172. Hoi, I.-C. et al. Demonstration of a single-photon router in the microwave regime. *Phys. Rev. Lett.* **107**, 073601 (2011).
  173. Geeraert, N., Bera, S. & Florens, S. Spontaneous emission of Schrödinger cats in a waveguide at ultrastrong coupling. *New J. Phys.* **19**, 023036 (2017).
  174. Geeraert, N. et al. Particle production in ultrastrong-coupling waveguide QED. *Phys. Rev. A* **98**, 043816 (2018).
  175. Goldstein, M., Devoret, M. H., Houzet, M. & Glazman, L. I. Inelastic microwave photon scattering off a quantum impurity in a Josephson-junction array. *Phys. Rev. Lett.* **110**, 017002 (2013).
  176. Meaney, C. P., Duty, T., McKenzie, R. H. & Milburn, G. J. Jahn-Teller instability in dissipative quantum systems. *Phys. Rev. A* **81**, 043805 (2010).
  177. Larson, J. Jahn-Teller systems from a cavity QED perspective. *Phys. Rev. A* **78**, 033833 (2008).
  178. Dereli, T., Güllü, Y., Forn-Díaz, P. & Müstecaplıoglu, Ö. E. Two-frequency Jahn-Teller systems in circuit QED. *Phys. Rev. A* **85**, 053841 (2012).
  179. Levine, G. & Muthukumar, V. N. Entanglement of a qubit with a single oscillator mode. *Phys. Rev. B* **69**, 112003 (2004).
  180. Hirokawa, M. The Rabi model gives off a flavor of spontaneous SUSY breaking. *Quantum Stud. Math. Found.* **2**, 379 (2015).
  181. Garziano, L., Stassi, R., Ridolfo, A., Di Stefano, O. & Savasta, S. Vacuum-induced symmetry breaking in a superconducting quantum circuit. *Phys. Rev. A* **90**, 043817 (2014).
  182. Gong, Z., Hamazaki, R. & Ueda, M. Discrete time-crystalline order in cavity and circuit QED systems. *Phys. Rev. Lett.* **120**, 040404 (2018).
  183. Ruggenthaler, M., Tancogne-Dejean, N., Flick, J., Appel, H. & Rubio, A. From a quantum-electrodynamical light-matter description to novel spectroscopies. *Nat. Rev. Chem.* **2**, 0118 (2018).
  184. Romero, G., Ballester, D., Wang, Y. M., Scarani, V. & Solano, E. Ultrafast quantum gates in circuit QED. *Phys. Rev. Lett.* **108**, 120501 (2012).
  185. Wang, Y., Guo, C., Zhang, G.-Q., Wang, G. & Wu, C. Ultrafast quantum computation in ultrastrongly coupled circuit QED systems. *Sci. Rep.* **7**, 44251 (2017).
  186. Stassi, R. et al. Quantum nonlinear optics without photons. *Phys. Rev. A* **96**, 023818 (2017).
  187. Stassi, R. & Nori, F. Long-lasting quantum memories: extending the coherence time of superconducting artificial atoms in the ultrastrong-coupling regime. *Phys. Rev. A* **97**, 033823 (2018).
  188. Kyaw, T. H., Felicetti, S., Romero, G., Solano, E. & Kwek, L.-C. Scalable quantum memory in the ultrastrong coupling regime. *Sci. Rep.* **5**, 8621 (2015).
  189. Nataf, P. & Ciuti, C. Protected quantum computation with multiple resonators in ultrastrong coupling circuit QED. *Phys. Rev. Lett.* **107**, 190402 (2011).
  190. Wang, Y., Zhang, J., Wu, C., You, J. Q. & Romero, G. Holonomic quantum computation in the ultrastrong-coupling regime of circuit QED. *Phys. Rev. A* **94**, 012328 (2016).
  191. Cao, X., You, J. Q., Zheng, H. & Nori, F. A qubit strongly coupled to a resonant cavity: asymmetry of the spontaneous emission spectrum beyond the rotating wave approximation. *New J. Phys.* **13**, 073002 (2011).
  192. Lizuain, I., Casanova, J., García-Ripoll, J. J., Muga, J. G. & Solano, E. Zeno physics in ultrastrong-coupling circuit QED. *Phys. Rev. A* **81**, 062131 (2010).
  193. Cao, X., Ai, Q., Sun, C.-P. & Nori, F. The transition from quantum Zeno to anti-Zeno effects for a qubit in a cavity by varying the cavity frequency. *Phys. Lett. A* **376**, 349 (2012).
  194. Seah, S., Nimmrichter, S. & Scarani, V. Refrigeration beyond weak internal coupling. *Phys. Rev. E* **98**, 012131 (2018).
  195. Felicetti, S., Romero, G., Rossini, D., Fazio, R. & Solano, E. Photon transfer in ultrastrongly coupled three-cavity arrays. *Phys. Rev. A* **89**, 013853 (2014).
  196. Lindner, N. H., Refael, G. & Galitski, V. Floquet topological insulator in semiconductor quantum wells. *Nat. Phys.* **7**, 490 (2011).
  197. Claassen, M., Jiang, H.-C., Moritz, B. & Devereaux, T. P. Dynamical time-reversal symmetry breaking and photo-induced chiral spin liquids in frustrated Mott insulators. *Nat. Commun.* **8**, 1192 (2017).
  198. Hübenr, H., Sentef, M. A., De Giovannini, U., Kemper, A. F. & Rubio, A. Creating stable Floquet-Weyl semimetals by laser-driving of 3D Dirac materials. *Nat. Commun.* **8**, 13940 (2017).
  199. Tame, M. S. et al. Quantum plasmonics. *Nat. Phys.* **9**, 329 (2013).
  200. Sentef, M. A., Ruggenthaler, M. & Rubio, A. Cavity quantum-electrodynamical polaritonically enhanced electron-phonon coupling and its influence on superconductivity. *Sci. Adv.* **4**, eaau6969 (2018).
  201. Schlawin, F., Cavalleri, A. & Jaksch, D. Cavity-mediated electron-photon superconductivity. Preprint at <http://arxiv.org/abs/1804.07142> (2018).
  202. Kockum, A. F., Macri, V., Garziano, L., Savasta, S. & Nori, F. Frequency conversion in ultrastrong cavity QED. *Sci. Rep.* **7**, 5313 (2017).
  203. Garziano, L., Stassi, R., Macri, V., Savasta, S. & Di Stefano, O. Single-step arbitrary control of mechanical quantum states in ultrastrong optomechanics. *Phys. Rev. A* **91**, 023809 (2015).
  204. Garziano, L. et al. Multiphoton quantum Rabi oscillations in ultrastrong cavity QED. *Phys. Rev. A* **92**, 063830 (2015).
  205. Ma, K. K. W. & Law, C. K. Three-photon resonance and adiabatic passage in the large-detuning Rabi model. *Phys. Rev. A* **92**, 023842 (2015).
  206. Garziano, L. et al. One photon can simultaneously excite two or more atoms. *Phys. Rev. Lett.* **117**, 043601 (2016).
  207. Ebbesen, T. W. Hybrid light-matter states in a molecular and material science perspective. *Acc. Chem. Res.* **49**, 2403 (2016).
  208. Bennett, K., Kowalewski, M. & Mukamel, S. Novel photochemistry of molecular polaritons in optical cavities. *Faraday Discuss.* **194**, 259 (2016).
  209. Kowalewski, M., Bennett, K. & Mukamel, S. Cavity femtochemistry: manipulating nonadiabatic dynamics at avoided crossings. *J. Phys. Chem. Lett.* **7**, 2050 (2016).
  210. Martínez-Martínez, L. A., Ribeiro, R. F., Campos-González-Angulo, J. & Yuen-Zhou, J. Can ultrastrong coupling change ground-state chemical reactions? *ACS Photonics* **5**, 167 (2018).
  211. Ruggenthaler, M. et al. Quantum-electrodynamical density-functional theory: bridging quantum optics and electronic-structure theory. *Phys. Rev. A* **90**, 012508 (2014).
  212. Schäfer, C., Ruggenthaler, M. & Rubio, A. Ab initio nonrelativistic quantum electrodynamics: bridging quantum chemistry and quantum optics from weak to strong coupling. *Phys. Rev. A* **98**, 043801 (2018).
  213. Chikkaraddy, R. et al. Single-molecule strong coupling at room temperature in plasmonic nanocavities. *Nature* **535**, 127 (2016).
  214. Ćwik, J. A., Kirton, P., De Liberato, S. & Keeling, J. Excitonic spectral features in strongly coupled organic polaritons. *Phys. Rev. A* **93**, 033840 (2016).
  215. Johansson, J. R., Nation, P. D. & Nori, F. QuTiP 2: a Python framework for the dynamics of open quantum systems. *Comput. Phys. Commun.* **184**, 1234 (2013).
  216. Chang, W.-H. et al. Efficient single-photon sources based on low-density quantum dots in photonic-crystal nanocavities. *Phys. Rev. Lett.* **96**, 117401 (2006).
  217. Raimond, J. M., Brune, M. & Haroche, S. Manipulating quantum entanglement with atoms and photons in a cavity. *Rev. Mod. Phys.* **73**, 565 (2001).
  218. Nataf, P. & Ciuti, C. Vacuum degeneracy of a circuit QED system in the ultrastrong coupling regime. *Phys. Rev. Lett.* **104**, 023601 (2010).

219. Rossatto, D. Z., Villas-Bôas, C. J., Sanz, M. & Solano, E. Spectral classification of coupling regimes in the quantum Rabi model. *Phys. Rev. A* **96**, 013849 (2017).
220. Rabi, I. I. Space quantization in a gyrating magnetic field. *Phys. Rev.* **51**, 652 (1937).
221. Xie, Q.-T., Cui, S., Cao, J.-P., Amico, L. & Fan, H. Anisotropic Rabi model. *Phys. Rev. X* **4**, 021046 (2014).
222. Hopfield, J. J. Theory of the contribution of excitons to the complex dielectric constant of crystals. *Phys. Rev.* **112**, 1555 (1958).
223. Gardiner, C. W. & Zoller, P. *Quantum Noise*, 3rd edn. (Springer, 2004).
224. Bamba, M. & Ogawa, T. Dissipation and detection of polaritons in the ultrastrong-coupling regime. *Phys. Rev. A* **86**, 063831 (2012).
225. Bamba, M. & Ogawa, T. Recipe for the Hamiltonian of system-environment coupling applicable to the ultrastrong-light-matter-interaction regime. *Phys. Rev. A* **89**, 023817 (2014).
226. Bamba, M., Inomata, K. & Nakamura, Y. Superradiant phase transition in a superconducting circuit in thermal equilibrium. *Phys. Rev. Lett.* **117**, 173601 (2016).
227. Bamba, M. & Ogawa, T. System-environment coupling derived by Maxwell's boundary conditions from the weak to the ultrastrong light-matter-coupling regime. *Phys. Rev. A* **88**, 013814 (2013).
228. De Liberato, S. Comment on "System-environment coupling derived by Maxwell's boundary conditions from the weak to the ultrastrong light-matter-coupling regime". *Phys. Rev. A* **89**, 017801 (2014).

#### Acknowledgements

Numerical simulations were performed using QuTiP<sup>215</sup>. The authors thank Y.-X. Liu, X. Gu, O. Di Stefano and A. Ridolfo for useful discussions. The authors also thank A. Settineri, M. Cirio and S. Ahmed for technical assistance with some of the figures. A.F.K. acknowledges partial support from JSPS Postdoctoral Fellowship for Overseas Researchers (P15750). A.M. and F.N. acknowledge support from the Sir John Templeton Foundation. S.D.L. acknowledges support from a Royal Society research fellowship and thanks F.N. for his hospitality at RIKEN during the course of this work. F.N. also acknowledges support from the MURI Center for Dynamic Magneto-Optics via the Air Force Office

of Scientific Research (AFOSR) award No. FA9550-14-1-0040, the Army Research Office (ARO) under grant No. W911NF-18-1-0358, the Asian Office of Aerospace Research and Development (AOARD) grant No. FA2386-18-1-4045, the Japan Science and Technology Agency (JST) through the Q-LEAP program, the ImPACT program, and CREST grant No. JPMJCR1676, the Japan Society for the Promotion of Science (JSPS) through the JSPS-RFBR grant No. 17-52-50023 and the JSPS-FWO Grant No. VS.059.18N, and the RIKEN-AIST Challenge Research Fund.

#### Author contributions

All authors researched data for the article, discussed the content, wrote the manuscript and reviewed and edited it before submission.

#### Competing interests

The authors declare no competing interests.

#### Publisher's note

Springer Nature remains neutral with regard to jurisdictional claims in published maps and institutional affiliations.